2007

Experimental Study Of Profiles Of Implanted Species Into Semiconductor Materials Using Secondary Ion Mass Spectrometry

Fatma Salman
University of Central Florida

EXPERIMENTAL STUDY OF PROFILES OF IMPLANTED SPECIES INTO SEMICONDUCTOR MATERIALS USING SECONDARY ION MASS SPECTROMETRY

by

FATMA SALMAN
B.S. Ain-Shams University, 1994
M. S. Ain-Shams University, 1999
M. S. University of Central Florida, 2003

A dissertation submitted in partial fulfillment of the requirements
for the degree of Doctor of Philosophy
in the Department of Physics
in the College of Sciences
at the University of Central Florida
Orlando, Florida

Summer Term
2007

Major Advisor: Lee Chow

ABSTRACT

The study of impurity diffusion in semiconductor hosts is an important field that has both fundamental appeal and practical applications. Ion implantation is a good technique to introduce impurities deep into the semiconductor substrates at relatively low temperature and is not limited by the solubility of the dopants in the host. However ion implantation creates defects and damages to the substrate. Annealing process was used to heal these damages and to activate the dopants.

In this study, we introduced several species such as alkali metals (Li, Na, K), alkali earth metals (Be, Ca,), transition metals (Ti, V, Cr, Mn) and other metals (Ga, Ge) into semiconductor substrates using ion implantation. The implantation energy varies form 70 keV to 200 keV and the dosages vary between ~ $1.0x10^{12}$ and ~$5.0x10^{15}$ atoms/cm^2. The samples are annealed at different temperatures from 300°C to 1000°C and for different time intervals.

The redistribution behaviors of the implanted ions are studied experimentally using secondary ion mass spectrometry (SIMS). We observed some complex distribution behaviors due to the defects created during the process of ion implantation. The diffusivities of some impurities are calculated and compared to previous data. It was found that the diffusivities of implanted impurities is related to the dosages, annealing temperatures and the defects and damages caused by ion implantation. Additionally, as we go from one type of semiconductor to another, the diffusion behavior of the impurities shows a different trend.

ACKNOWLEDGMENTS

I would like to thank Dr. Lee Chow for caring, supporting, and the great guidance over the years. I also appreciate the help and support of Dr. Gabriel Braunstein and Dr. Robert Peal. I gratefully acknowledge Mr. Michel Klimov for the SIMS measurements. Most of all, I want to thank from the bottom of my heart my husband, Dr. Mohamed Ghonaim, my kids Nouran, Sarah, and Kareem and my parents for showing the patience, love, support, and care for so many years.

TABLE OF CONTENTS

LIST OF FIGURES

LIST OF TABLES

CHAPTER 1
GENERAL INTRODUCTION

In this study, we introduced many elements into semiconductor substrates. These elements including alkali metals (Li, Na, K), alkali earth metals (Be, Ca,), transition metals (Ti, V, Cr, Mn) and other metals (Ga, Ge) are implanted into silicon (Si), poly-silicon (poly-Si), silicides ($TaSi_2$) and Gallium Nitride (GaN) substrates. Ion implantation method was used for the doping process. The implantation energy varies form 70 keV to 200 keV and the dosages vary between ~ $1.0x10^{12}$ to ~$5.0x10^{15}$ atoms/cm^2. The samples are annealed at different temperatures from 300°C to 1000°C and at different time intervals. The distribution behavior of the implanted and annealed dopants is studied experimentally using Secondary Ion Mass Spectrometry (SIMS).

The goal of this work is to study the behavior of impurities inside semiconductors; where it is well established that the diffusion of impurities even at very low concentration, can affect the electronic properties. As the semiconductor devices get smaller and smaller, impurities in the active device region get more significant role. In general, impurities can be introduced into semiconductors using two main techniques: thermal diffusion and ion implantation. Thermal diffusion is a common method that has been used for the past 30 years. However, this process requires elevated temperatures, and it is delimited by the solubility in the host. We used ion implantation to introduce impurities into semiconductor substrates. Ion implantation is a good technique to introduce dopants deep into the substrate at low temperature and it doesn't depend on the solubility limit. However ion implantation creates crystal damages. Annealing process has been used to heal these damages and to activate the dopants

The dissertation includes 8 chapters, arranged as the following: chapter 1: A general introduction. Chapter 2: A review of the basic concepts and theories of ion implantation as a doping technique. Chapter 3: A detailed revision of the Secondary Ion Mass Spectrometry (SIMS) as a technique that was used to characterize the distribution profile of the dopants in semiconductor materials. Chapter 4: Study of the diffusion phenomena in silicon, poly-silicon and silicides. Starting from chapter 5, The experimental procedures and results of low dosages Chromium (Cr) and Vanadium (V) implanted into crystalline silicon substrates are studied. Chapter 6: The diffusion of implanted species in poly-silicon films on silicon substrates is investigated. Chapter 7 and 8 are dealing with the annealing behavior of implanted elements in tantalum silicide ($TaSi_2$) and the annealing behavior of implanted Lithium (Li) ions in Gallium Nitride (GaN) thin films.

CHAPTER 2
ION IMPLANTATION

2.1. Introduction

Ion implantation is a common method used to introduce impurities into a substrate. In this process, molecules or atoms are ionized, accelerated, and implanted into a solid. The acceleration energy can vary from keV to MeV and the dosage level can vary form 10^{12} cm^{-2} to 10^{16} cm^{-2}. In this section, we will review the advantages and the disadvantages of ion implantation as a method of doping impurities into semiconductors, in addition to the review of some characteristics of ion implantation, such as distribution, channeling and ion range. Refer to [RYSS86, ZIEG88] for more detailed discussion about ion implantation method.

2.1.1. The advantages and disadvantages of ion implantation for doping

Using ion implantation gives many advantages, first, the ions of the dopant can be introduced at temperatures at which normal diffusion can be neglected. This property is very important for co-implantation, in this way, the profiles of the previously doped dopants will not be disturbed. Another advantage of ion-implantation is that the implanted ions are controlled by an external system so it doesn't depend on the properties of the substrate such as the solubility limit. It doesn't depend on the concentration of the dopant at the surface of the semiconductors which it can't be done in the case of thermal diffusion as another method to introduce dopants into substrates. These aspects and even more make ion implantation is the most dominant method to introduce dopant into semiconductor substrates. Table 2.1 shows some advantages and also limitations for the ion implantation method.

Table 2.1. The advantages and limitations of ion implantation for doping.

Advantages	Limitations
Almost all elements can be implanted	Relatively expensive
Controlled dosage	Can damage the substrate
Controlled depth profile	Annealing is required to heal the damage
Low temperature	Difficult to achieve very shallow profiles
Good reproducibility of the profiles	Difficult predict the exact profile shapes
Short time process	Change the material properties restricted to the surface
Can exceed the solid solubility limit	
Low penetration depth, thus no sacrifice of bulk properties	
Multiple implantation	

In the normal thermal diffusion process, the dopants diffuse from the surface into the substrate. The dose diffused is influenced by the surface condition. The diffusion profile follows the complementary error function. In this case, the concentration depth profile is difficult to control. As a contrast, ion implantation can accurately control the concentration distribution by changing implantation energies. However, the energetic processes, especially those of high dosage and high energy, generate damages and thermal treatment, *annealing*, is needed to activate the dopants. During the annealing, the near surface impurities may diffuse deep into the substrate and at the same time, the dopant profiles will extensively expand. This makes it difficult to shrink the size of devices. Therefore, it is important to understand the behavior of damage during annealing and the behavior of impurities in the semiconductor devices.

2.2. Basic Concepts and theoretical background for Ion Implantation

2.2.1. Fundamentals of ion-solid interactions

When an ion with a high velocity strikes a solid, the incident ion will transfer all or some of its energy to the solid. The transferred energy depends on many factors such as the masses of the target nuclei and the incident ion, the energy and the angle of the incident ion. For example, if the energy of the incident ion is less than 100 eV, the ion will stop on or near the surface, in this way, it is useful to build thin films. If the incident ion energy is between 1-20keV, the energy will transfer from the incident ion to the target nuclei, which cause sputtering and the removal of surface layers. At higher energy (100-300keV), ions will be implanted into the solid substrates.

Table 2.2. Energy ranges and different applications of ions.

Energy	Applications
~10-100eV	Ion beam deposition
~1keV	Sputtering
~keV-MeV	Ion Implantation
~1MeV	Ion Beam Analysis
Higher energies	Resonance Analysis and Nuclear reaction Analysis etc. [BREE96]

The ions can penetrate deeply into the solid (microns) with MeV energy [HOLL96]. Table 2.2 lists the applications of ions in different energy levels. For the energy range keV ~ MeV [CHU78], the collisions between incident particles and the target atoms can be well described by single binary elastic collision theory. This is based on two assumptions: (1) the energy E_0 of incident ion should be much larger than the binding energy (of the order 10eV) of the atoms in the target. (2) No nuclear reaction and resonance. Therefore, the *Kinematic factor k* (the ratio of

the projectile energy after collision to the incident energy of the ion before collision) and scattering cross section $d\sigma/d\Omega$ (the measure of the effectiveness of the projectile-target interaction over a certain area) can be calculated with this theory, for more details, see [CHU78].

2.2.2. Energy Losses, Ion Ranges and Ion Range Distribution

The ion range or the energy loss of an ion can be determined by many factors, these include its energy E, atomic number Z_1 of the impinging ion, and the atomic number Z_2 of the substrate. Furthermore, the *orientation* of the sample (channeling effect) and the vibration (temperature-determined) of the lattice atoms are also important [MAYE70]. The energy loss of ion moving through solid matter at keV energy is determined by the screened Coulomb interactions with the substrate atoms. The two main processes of energy loss are; (1) The interactions of the moving ion with the electrons (inelastic collision or elastic collision) in the target, and (2) the interactions of the moving ion with the nuclei (elastic collision) of the target atoms [CHU78, ZIEG85].

Figure (2.1) represents the energy loss ($dE/d\chi$) as a function of the projectile energy where ε_n is the nuclear stopping power, ε_e is the electronic stopping power. The dashed lines show the limits for Lindhard, Scharff and Schiøtt theory (LSS theory or low energy) and the Bethe-Bloch theory (high energy) [MAYE70, CHU78 and MILL93].

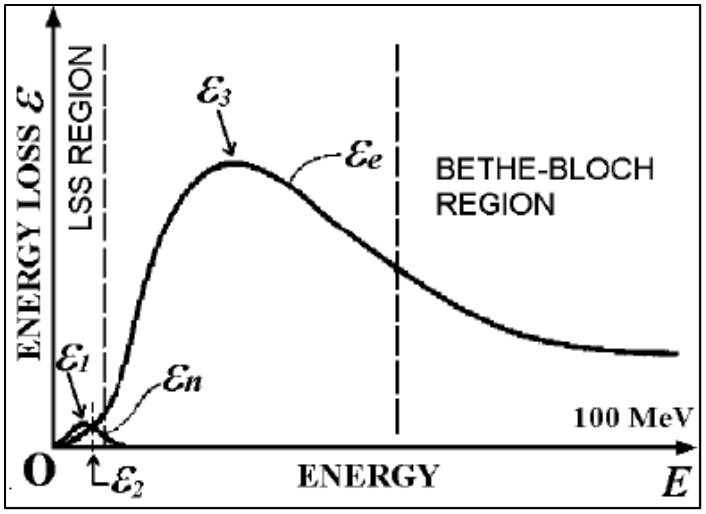

Figure 2.1. Plot of the energy stop cross section as a function of energy. [MAYE70]

The energy-loss rate ($dE/d\chi$) is expressed as:

$$\frac{dE}{dx} = \frac{dE_e}{dx} + \frac{dE_n}{dx} \tag{2.1}$$

The nuclear collision involves more energy loss and the electronic collision involves less energy loss. In addition to the energy loss rate we should mention the stopping cross section S, where:

$$S = \frac{1}{N}\frac{dE}{dx} \tag{2.2}$$

where N is the atomic density.

The total distance (range) of the incident ion can be calculated:

$$R = \int_0^E \frac{dx}{dE} dE = \int_0^E \left(\frac{dE}{dx}\right)^{-1} dE \tag{2.3}$$

In ion implantation process, not only the total distance R traveled by implanted ion is of interest but also the projection of R normal to the surface (R_p) as shown in fig. (2.2).

The range of ion by LSS theory is the total distance *R* that the ion travels before it comes to rest. If the nuclear collision is dominant then another, then another rule such as a rough *rule of thumb* $\frac{R}{R_P} = 1 + \frac{M_2}{3M_1}$ [MAYE70] is applied, where M_1 and M_2 are the masses of the projectile and the target respectively. In this case, the mass of the incident ion should be greater than the mass of the target ($M_1 > M_2$), within reasonable range for M_1 and M_2

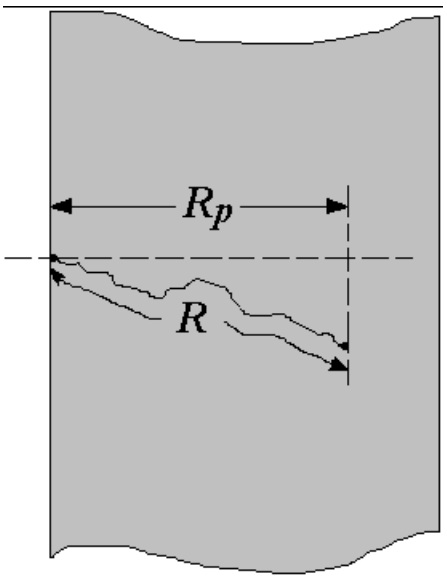

Figure 2.2. Schematic diagram illustrates the range R and the projection range Rp. [MAYE70]

Each ion introduced to the target will not travel precisely the same path, even though the initial energy is fixed. Owing to different random impact parameters of the ions. Therefore, they will have different ranges, resulting in a distribution of stopping positions. The stopping positions are assumed to have a Gaussian distribution peaked at the depth R_p [CART76]:

$$N(x) = \frac{0.4N_s}{\Delta R_p} \exp\left[-\frac{1}{2}\left(\frac{x - R_p}{\Delta R_p}\right)^2\right] \tag{2.4}$$

Where N_s is the number of implanted ions per unit area (dosage) and ΔR_p is the standard deviation.

Since 1960's, Computer simulation methods have been developed to determine the range and the distribution of ions in a solid. Silicon received the most attention as a medium. The basic idea in those methods is to follow the pathway of the ion in the medium by simulating the collisions with nuclei in the solid. The electronic stopping power is usually taken into account as a frictional force slowing down the ion. Generally, there are three different kinds of models which could be used to simulate the ion-solid interaction: Binary Collision Approximation (BCA) [JARA96, CHAS97]; classical molecular dynamics [RUBI95, REED98 and YAMA99], and quantum mechanical method [TANG97]. In the BCA method, the movement of ions in the implanted sample is treated as a succession of individual collisions between the recoil ion and atoms in the sample. The best known simulation program is SRIM (The Stopping and Range of Ions in Matter) [PIER80, ZIEG85], available for download at J. F. Ziegler's homepage (http://www.research.ibm.com). SRIM is a group of programs which calculate the stopping and range of ions (energy between 10eV-2GeV) into matter using a quantum mechanical treatment of ion-atom collisions. The full description of the calculation is in [ZIEG85].

2.2.3. Channeling

The Stopping and Range of Ions in Matter (SRIM) is a very useful tool to determine the range or the distribution of the ions if we ignored the orientation, i.e. it assumes that the target is amorphous. In crystalline materials the ion may in some instances get "channeled", i.e. get

focused into a channel between crystal planes or major axes (e.g.,<110>,<111> ,<100>) where there are practically no nuclear collisions with nuclei; so the stopping only takes place due to the electronic collision. However, the electronic stopping power may be weaker in the channel [FELD86]. The crystalline BCA codes intentionally describe channeling effects. Though, in order to take into account the weaker electronic stopping in simulations, one must use a non-local electronic stopping power, i.e. the one that depends on the strength of the collisions the ion experiences. The channel potential distribution can explain the trajectories of ions into single crystal [CART76]. The channeling effect also plays an important role in SIMS analysis [THOM76, CHU78, FELD82 and FELD86]. Fig. 2.3 (a) represents a model for diamond lattice structure along <110> axis and fig. 2.4 (b) is representing a random direction at ~10° from <110> direction.

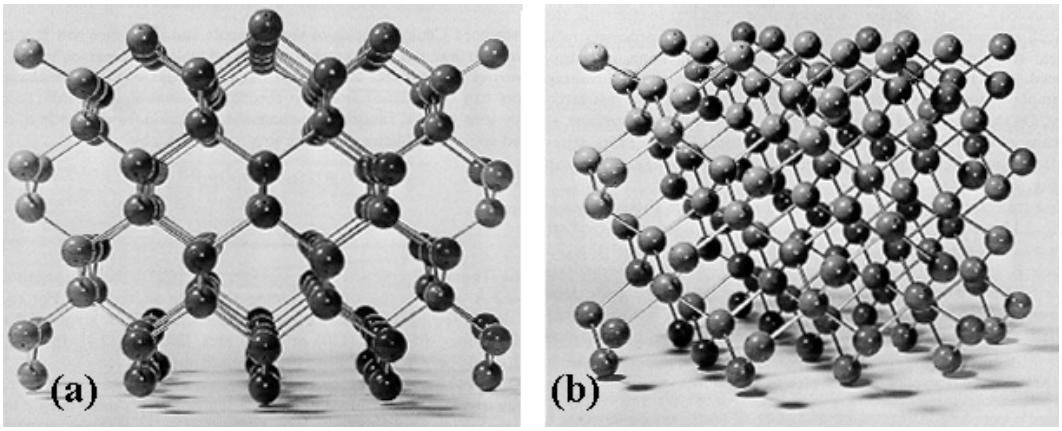

Figure 2.3. Diamond-type lattice viewed along (a) <110> axis, and (b) viewed along a "random" .direction at ~10° from <110> direction. [MAYE70].

2.3. Defects and Lattice Disorder Formed by Ion Implantation

It is important to understand the associated defects with ion implantation because of the extensive use of it in the semiconductor technology and the shrinking in the scale. When ions

with high energy collide with the substrate, atoms are displaced from their lattice sites and produce many types of defects such as *vacancy*, *interstitial*, and *interstitialcy*, etc. [CART76, CHAS97]. Some authors classified implantation defects into five categories, such as *dislocation*, *clusters*, *vacancy*, *intestinal* and *interstitialcy*, for more details, see [JONE88].

At equilibrium, the atom is bound to fixed lattice sites by the interaction forces with its neighbors. After ion implantation, the atom receives enough energy from collision, which can break the binding forces. The atom leave the equilibrium position and a *vacancy* is created in the lattice. If this atom finally stops in a non-lattice position, an *interstitial* is also created. The implanted ions can also be *interstitials* if they are not at the lattice sites. The rate of *vacancy* formation follows the relation $v = v_0 \exp\left(\frac{-E_v}{kT}\right)$, where E_v is the energy needed to form *vacancy*. The rate of forming *interstitial* follows the same relation $I = I_0 \exp\left(\frac{-E_i}{kT}\right)$, where E_i is *interstitial* formation energy. It was found that for Germanium (Ge) and Si hosts, the *vacancy* formation energy (E_v) is around 2.0 eV and the energy needed to form *interstitial* is between 4-5 eV [CART76].

The solid will change from *ordered* to *disordered* if lots of *vacancies* and *interstitials* are formed. If the energy and the dosage of implanted ions are high enough, the ions can transform the top of the crystalline substrate into an amorphous layer [RYSS86]. For example, heavy ions implanted at room temperature and dosage above 10^{14} cm^{-2} can produce an amorphous layer

under the surface and the thickness of this layer depends on the implanted ion beam energy [RIMI95].

Theoretically, the host damage formed by ion implantation is simulated by SRIM/TRIM. Other simulation programs such as Monte Carlo ion implantation simulation and quantum mechanical method, are detailed in [TIAN98, BOHM98, POSS99 and CHAK01]. Others [HIRV80, FELD82, JONE88, CHAS97, CART76, BEHR76 and CHU78] used experimental techniques such as Transmission Electron Microscope (TEM), Rutherford Back Scattering (RBS), Field Ion Microscopy (FIM) and Reflection Electron Diffraction (RED), to characterize the damage and the epitaxial growth.

When the implanted sample is annealed, the amorphous layer starts to recrystallize with a velocity that depends on temperature, dopant, and the orientation of substrate [CSEP78, HO84, RYSS86 and OLSO88]. The growth velocity v_g can be measured using the following formula [CSEP78]; $\nu_g = \nu_0 \exp\left(\frac{-E_A}{kT}\right)$, where E_A = 2.76 eV and v_0 = 3.68x10^6 m/s. Fig. (2.4) illustrates the relation between solid phase epitaxial regrowth velocity and temperature. The regrowth of the amorphous layer is believed to occur with the motion of the amorphous/crystalline (a/c) interface but not the nucleation of new crystals within the amorphous layer [DROS82].

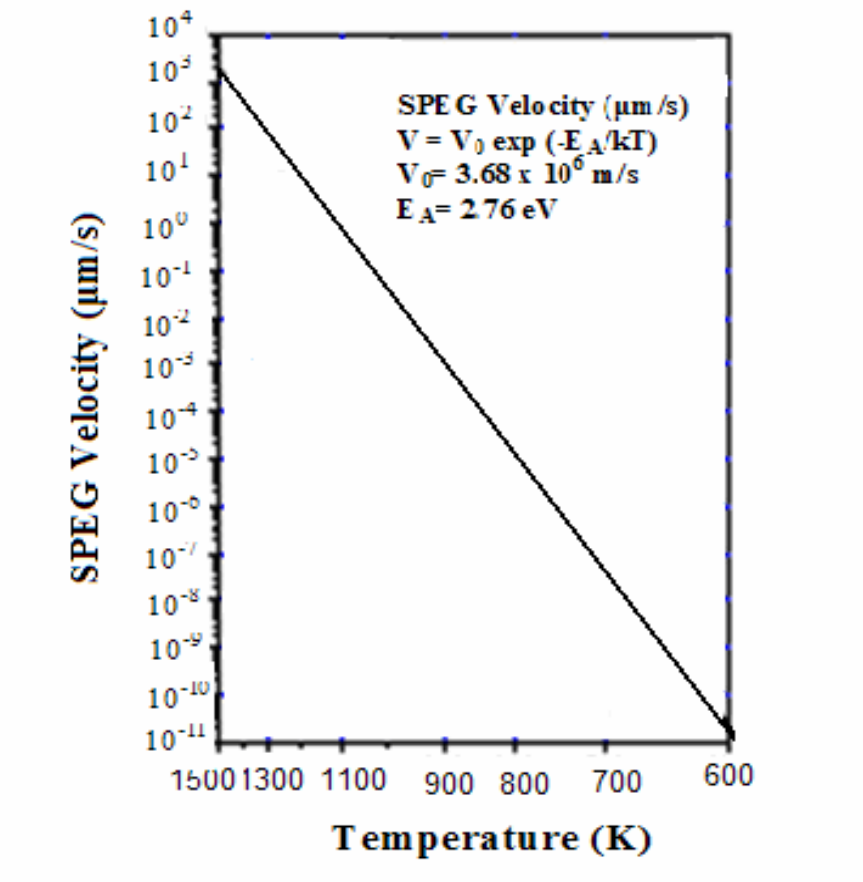

Figure 2.4. Solid phase epitaxial regrowth of implanted amorphous silicon on Si (100) substrate [CSEP78]

2.4. References

[BEHR76] R. Behrisch and J. Roth, Depth Distribution of Damage Obtained by Rutherford Backscattering Combined with Channeling, in Ion Beam Surface Layer Analysis, edited by O. Meyer, G. Linker and F. Käppeler, Academic Press (1976).

[BOHM98] W. Bohmayr, A. Burenkov, J. Lorenz, H. Ryssel and S. Selberherr, IEEE Transactions on Computer-*Aided Design* **17**, 1236 (1998).

[CART76] G. Carter and W. A. Grant, *Ion Implantation of Semiconductors*, John Wiley & Sons (1976).

[CHAK01] S. Chakravarthi, S. T. Dunham, J. Appl. Phys. **89**, 4758 (2001).

[CHAS97] E. Chason, S. T. Picraux, J. M. Poate, J. O. Borland, M. I. Current, T. Diaz de la Rubia, D. J. Eaglesham, O. W. Holland, M. E. Law, C. W. Magee, J. W. Mayer, J. Melngailis and A. F. Tasch, J. Appl. Phys. **81**, 6513 (1997).

[CHU78] W. K. Chu, J. W. Mayer and M-A. Nicolet, *Backscattering Spectrometry*, Academic Press (1978).

[CSEP78] L. Csepregi, E. F. Kennedy, J. W. Mayer and T. W. Sigmon, J. Appl. Phys. **49**, 3906 (1978).

[DROS82] R. Drosd and J. Washburn, J. Appl. Phys. **53**, 397 (1982).

[FELD82] L. C. Feldman, J. W. Mayer and S. T. Picraux, *Materials Analysis by Ion Channeling*, Academic Press (1982).

[FELD86] L. C. Feldman and J. W. Mayer, *Fundamentals of Surface an Thin Film Analysis*, North-Holland (1986).

[HIRV80] J. K. Hirvonen, p. 1-16 in *Treatise on Materials Science and Technology* edited by J. K. Hirvonen, Academic Press (1980).

[HO84] K. T. Ho, I. Suni, and M-A. Nicolet, J. Appl. Phys. **56**, 1207 (1984).

[HOLL96] P. Holloway and G. McGuire, Handbook of Compound Semiconductors: Growth, Processing, Characterization, and Devices. (1996), p.655.

[JARA96] M. Jaraiz, G. H. Gilmer, J. M. Poate, and T. D. de la Rubia, Atomistic Calculations of Ion Implantation in Si: Point Defect and Transient Enhanced Diffusion Phenomena, Appl. Phys. Lett. **67**, 409 (1996).

[JONE88] K. S. Jones, S. Prussin and E. R. Weber, Appl. Phys. A **45**, 1 (1988).

[MAYE70] J. W. Mayer, L. Eriksson and J. A. Davies, *Ion Implantation in Semiconductors - Silicon and Germanium*, Academic Press (1970).

[MILL93] A. C. Miller, R. B. Irwin and H. F. Helbig, *Low-Energy Ion Scattering And Rutherford Backscattering Spectroscopies*, in *Physical Methods of Chemistry* (Vol.9B), 2nd edition, John Wiley & Sons (1993).

[OLSO88] G. L. Olson and J. A. Roth, Material Science Reports **3**, 1 (1988).

[PIER80] J. P. Biersack and L. Haggmark, Nuclear Instruments and Methods **174**, 257 (1980).

[POSS99] M. Posselt, International Conference on Ion Implantation Technology Proceedings, IEEE (1999).

[REED98] K. M. Beardmore and N. G. Jensen: http://europa.das.ucdavis.edu/~reed/reed.shtml.

[RIMI95] E. Rimini, *Ion Implantation: Basics to Device Fabrication*, Kluwer Academic Publishers (1995).

[RUBI95] T. Diaz de la Rubia and G. H. Gilmer, Phys. Rev. Lett. **74**, 2507 (1995).

[RYSS86] H. Ryssel and I. Ruge, *Ion Implantation*, John Wiley & Sons (1986).

[TANG97] M. Tang, L. Colombo J. Zhu and T. Diaz de la Rubia, Phys. Rev. B **55**, 14279 (1997).

[THOM76] J. P. Thomas and A. Cachard, *Material Characterization Using Ion Beams*, Plenum Press (1976)

[TIAN98] S. Tian, M. F. Morris, S. J. Morris, B. Obradovic, G. Wang, A. F. Tasch and C. M. Snell, **45**, 1226 (1998).

[YAMA99] Y. Yamamura, T. Kenmotsu, K. Yorizane and T. Muramoto, International Conference on Ion Implantation Technology Proceedings, IEEE (1999).

[ZIEG85] J. F. Ziegler, J. P. Biersack and U. Littmark, *the Stopping and Range Of Ions In Solids*, Pergamon (1985).

[ZIEG88] J. F. Ziegler edited, Ion Implantation Science and Technology, Academic Press (1988).

CHAPTER 3
SECONDARY ION MASS SPECTROMETRY (SIMS) INSTRUMENTATION

3.1. Introduction

The surfaces and the near- surface areas (~ 0.1 μm) play an important role in semiconductor industries as the size of the semiconductor devices keeps shrinking. There are many ways to analyze the surface of devices [MILL93]. Powell gave a list of these techniques [POWE78]. Secondary Ion Mass Spectrometry (SIMS) is one of these techniques and is the one used in this work to characterize the distribution of impurities in semiconductors.

Secondary Ion Mass Spectrometry (SIMS) is used to quantify and identify contaminations in thin films. SIMS is the mass spectrometry of atomic or molecular ions which are emitted due to bombarding the substrate with primary energetic particles [BRIG89]. The detected secondary ions may be emitted from the surface in the ionized state or emitted as neutrals to be post-ionized before analysis. Therefore, any SIMS apparatus include a primary ion source, a vacuum chamber to place the specimen under study in, a mass analyzer, and a secondary ion detector. SIMS is a destructive technique because it relies on particle removal from the surface. However, the advantage of SIMS comes from the high sensitivity and excellent depth resolution which makes it widely used for analysis of trace elements in solid materials, especially semiconductors but it could be also applied for any type of materials such as insulators, metals and organic molecules that can stay under vacuum [FELD86, CHAS97 and SCHR98].

3.2. SIMS Measurements and Depth Resolution

There are many parameters that can affect SIMS depth resolution, these are: The impact energy, the primary beam species, the primary ion angle of incidence, the sputtering rate, and the ratio of the detected area and the rastered area [CHER87].

Depth resolution is affected by changing of the primary ion beam species. A lighter ion beam can give better depth resolution profile because it penetrates deeper into the substrate, in contrary to a heavier primary ion beam which can penetrate only into a shallower region from the surface. The depth resolution increases as the impact energy decreases. Additionally, depth resolution can be affected by the angle of incidence of the primary ion beam. The optimum depth resolution is reached at off normal incidence because the collision cascade in the sputtering process occurs closer to the substrate surface than at the normal incidence. Furthermore, the poor depth resolution may be due to the increase of the sputtering rate. As previously mentioned, the raster size is also playing a role on depth resolution, for more details, see [CHER87].

The sputtering of the particles and the ionization of the particles are two main processes involved in SIMS measurements. In order to describe the Secondary Ion Emission process (SIE), many parameters or coefficients is defined as the following [CHER87]: (1) SIE coefficient $K_i^+ = N_i^+ / N_o$ where N_i^+ is the number of the positive secondary ions and N_o is the number of the primary ions. (2) The secondary ion yield $\gamma_i^+ = K_i^+ / C_i$ where C_i is the concentration of the i^{th} component. (3) The sputtering coefficient $S = N/N_o$ where N is the total number of the sputtered

particles. (4) The ionization probability $R_i^+ = K_i^+ / S$ which it varies from 0 to 1. (5) The ionization degree $\beta_i^+ = N_i^+ / N^o$ where $N°$ is the number of neutral particles.

In general, there are several modes of SIMS instrument operations: Static, dynamic, ion imaging, and isotope ratio measurement, each of which yields a special information and analytical features. SIMS static type uses low primary ion current while Dynamic SIMS uses a high primary ion current density on the sample. Thus, dynamic SIMS has a much higher sputter rate (~10μm/hour) than that of static SIMS (~ 0.1nm/hour) [SCHR98]. More information about the static SIMS type is given in [VICK98, VAEC99 and ADRI99]. The static SIMS is used for surface chemical characterization which gives information about the atoms in the upper monomolecular layer of the sample [BERN87]. In order to obtain the depth profiles of impurities implanted into semiconductors, dynamic SIMS is used in our work to provide the depth distribution of the trace elements. The analyses were carried out in Material Characterization Facility (MCF) at the University of Central Florida with a CAMECA IMS-3f with a 10 keV O_2^+ as a primary ion beam. Detailed parameters and descriptions of CAMECA IMS-3f are given in the following table 3.1 and fig. (3.1) In CAMECA IMS-3F, an O_2^+ primary beam was used to increase positive secondary ion yield. The primary ion beam energy and current have to be chosen very carefully because high energy can cause depth profile distortion. High beam current can cause fast sputtering and depth profile distortion. On contrast, too low beam current can cause slow sputtering which will take a long time to acquire a depth profile.

Table 3.1 Characteristics of SIMS; CAMECA IMS-3f.

Depth resolution	~5nm
Mass resolution (M/ΔM)	From 200 to more than 1000
Mass range	0-250 amu
Primary ions	O_2^+, O^-, Ar^+, Xe^+, Cs^+ from 5 to 15 V
Maximum sample size	1*1*1 cm^3
Mass analyzer type	Magnetic sector

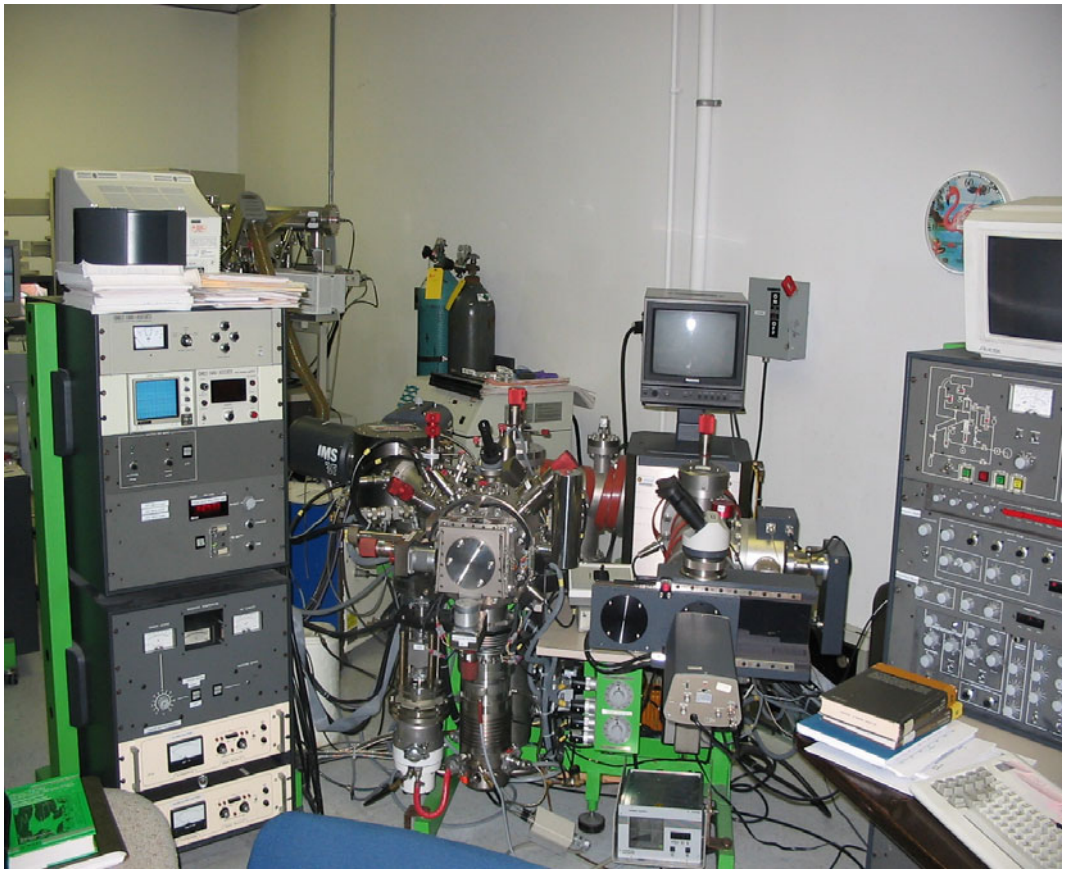

Figure 3.1. University of Central Florida SIMS; AMECA MS-3f.

Another mode of SIMS instrument operation is ion imaging which allows lateral imaging, It can give 3D compositional reconstruction for heterogeneous sample if combined with depth profiling. Isotope ratio measurement is another unique application of SIMS which can be used to measure isotope ratio with precision of at least 0.1%.

3.3. References

[ADRI99] A. Adriaens, L. V. Vaeck and F. Adams, Mass Spectrometry Reviews **18**, 48 (1999).

[BERN87] M. T. Bernius and G. H. Morrison, Review of Scientific Instruments **58**, 1789 (1987).

[BRIG89] D. Briggs, A. Brown and J. Vickerman, *Hand Book of Static Secondary Ion Mass Spectrometry*, John Wiley & Sons (1989).

[CHAS97] E. Chason, S. T. Picraux, J. M. Poate, J. O. Borland, M. I. Current, T. Diaz de la Rubia, D. J. Eaglesham, O. W. Holland, M. E. Law, C. W. Magee, J. W. Mayer, J. Melngailis and A. F. Tasch, J. Appl. Phys. **81**, 6513 (1997).

[CHER87] V. T. Cherepin, *Secondary Ion Mass Spectrometry of Solid Surface*, academic press (1987).

[FELD86] L. C. Feldman and J. W. Mayer, *Fundamentals of Surface an Thin Film Analysis*, North-Holland (1986).

[MILL93] A. C. Miller, R. B. Irwin and H. F. Helbig, in Physical Methods of Chemistry (Vol.9B), 2nd edition, John Wiley & Sons (1993).

[POWE78] C. J. Powell, Applied Surface Science **1**, 143 (1978).

[SCHR98] D. K. Schroder, *Semiconductor Material and Device Characterization*, John Wiley & Sons (1998).

[VAEC99] L. V. Vaeck, A. Adriaens and R. Gijbels, Mass Spectrometry Reviews **18**, 1 (1999).

[VICK98] J. C. Vickerman, p.71 *in Spectroscopy for Surface Science edited by* R. J. H. Clark and R. E. Hester, John Wiley & Sons (1998).

CHAPTER 4
DIFFUSION IN SILICON

Silicon is a semiconductor material that is widely used. The crystal structure for silicon is diamond cubic structure [MAYE70], which can be looked as of two interpenetrating face-centered cubic lattices. Fig. 4.1 shows the diamond cubic lattice type.

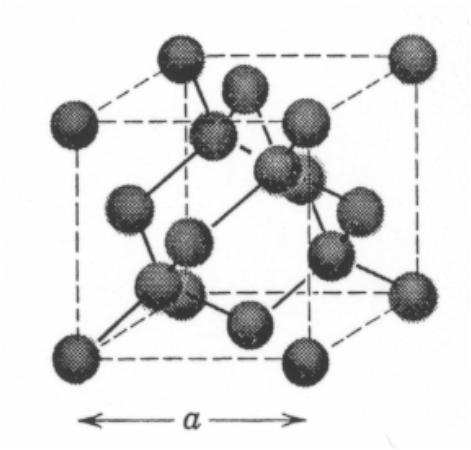

Figure 4.1. Diamond lattice structure for silicon.(http://www.imit.kth.se/)

In our work, we used single crystal silicon (100). Single crystal means that there is a periodic arrangement of atoms, which make up the solid throughout the crystal [WOLF00]. The huge demand on the study of diffusion in semiconductor materials comes from the technical significance of the diffusion process step for integrated circuit (IC) fabrication. Modern process technologies try to reduce unwanted and unpredictable diffusion phenomena by performing short term annealing at high temperatures or by reduction of the annealing temperature.

There are many ways to introduce dopants into semiconductors. Currently, ion implantation is the main tool to introduce dopants into semiconductors mentioned in chapter 2. By controlling

the dopants of impurity atoms, the properties of silicon-based devices and materials can be changed. Ion implantation will generate different types of damage [JONE88] in silicon, which leads the system to be far from equilibrium. To heal these damages, annealing is used to electrically activate the sample and bring the system closer to its equilibrium condition. During the annealing process, the impurity atoms are activated and at the same time dopants will diffuse in the bulk of the substrate. In this chapter we will study the diffusion behavior of transition metals such as V and Cr in Si. The significance of such study is because the diffusion of transitional metal impurities such as Fe and Cu etc., are harmful to the devices [MYER00]. In other words, for 0.1μm technology, a *single* Fe atom segregated to the gate oxide can kill the transistor [DABR99]. Therefore, it become increasingly crucial to be able to understand the diffusion behavior of transition metals during the fabrication process of semiconductor devices. Nevertheless, the diffusion of transition metals is very complicated process [HU73, FAHE89, CHAS97] because of the deformations and defects such as *interstitials* , [BRAC91]*vacancies* [LIST98, BUNE00] and *clusters* [RAFF96, CHAK01] etc. Any impurities doped into silicon is subjective to the point defects, Consequently, it is important to discuss the properties of the point defects in silicon.

4.1. Point Defects in Silicon

The impurity diffusion is correlated to the interactions between point defects and impurities. For point defect, there are two categories: Native point defects exist in pure silicon lattice and impurity-related defects due to the introduction of impurities into silicon. Equilibrium defect concentration, migration are detailed in the following section.

4.1.1. Native Point Defects

There are three types of native point defects: *vacancies*, *interstitials*, and *interstitialcies.* These defects, always exist in silicon under equilibrium condition. They can develop and form extended defects such as {311} defect, Transient Enhanced Diffusion (TED) [EAGL94, JARA96 and CHAS97], and Oxidation Enhanced Diffusion (OED) [FAHE89, DUNH92 and GOSS93].

Vacancy is formed due to the removal of an atom from the lattice site; *interstitial* is formed when silicon atom is resided in one of the interstices of the silicon lattice. *Interstitialcy* is formed by placing an extra atom about the lattice site. There is also *extended point defect* [SEEG68], which means that the defect is not limited to a small area. According to statistical physics, under thermal equilibrium, point defects always exist once the temperature is above 0 K. The destruction of the perfect silicon lattice increases the free energy, while the existence of point defects increases the randomness (entropy) and decrease the free energy. The equilibrium concentration C_x^* of point defect *x* is expressed as in equation (4.1) and (4.2):

$$C_x^* = \theta_x C_s \exp(-\frac{G_x^f}{kT}) \quad (x = I, V) \tag{4.1}$$

$$G_x^f = H_x^f - T \cdot S_x^f \tag{4.2}$$

where θ_x is the internal degrees of freedom such as spin. C_S is the concentration of available lattice sites in the crystal. H_x^f and S_x^f are the formation enthalpy and entropy, T is the lattice temperature and k is Boltzmann constant. The formation energies and entropies can be calculated theoretically [SWAL73, BLÖC93 and CLAR97], but there is inconsistency about the formation

energies between different authors and between the experimental results and theoretical calculations [HU73, FAHE89].

4.1.2. Impurity-related Defects

In the recombination processes such as (Frank-Turnbull recombination), impurity-defect pairs recombine at lattice sites. The substitutional defect occurs when an impurity atom is located on a lattice site. Almost all of the dopant atoms dissolve in the lattice on substitutional lattice sites. The dopant defects can migrate in the AV, AI or A_i, modes, where AV represents the *dopant-vacancy pair*, AI is representing *dopant-interstitialcy pair*. If the dopant atoms itself occupies an interstitial position, it will be referred to as an interstitial dopant and is written as A_i. Where A is referring to a dopant atom and V is referring to a vacancy. The dopant defects are formed by the reactions

$$A+V \Leftrightarrow AV$$
$$A+I \Leftrightarrow AI$$
$$A+I \Leftrightarrow A_i$$
$$A \Leftrightarrow A_i+V$$

4.1.3. Sources and Sinks for Point Defects

At thermal equilibrium, concentration of point defects is calculated using fundamental thermodynamic principles. But these concepts give no information about how equilibrium is reached and what are the processes that generate or annihilate point defects in silicon. In dislocation-free silicon crystal, there are only two possibilities [FAHE89]. One possibility is when silicon atoms spontaneously creating *vacancy* and *interstitial* point defects; this process is

reversible (4.3). It is known as *Frenkel pair process* when point defects are formed and as *bulk process* when point defects recombined, see fig. (4.2).

$$I + V \Leftrightarrow 0 \tag{4.3}$$

Under thermal equilibrium the number of *vacancies* and *interstitials* is not necessary to be equal as long as both of the species can recombine at the surface. The local dynamic equilibrium is expressed as (4.4):

$$C_I \times C_V = C_I^* \times C_V^* \tag{4.4}$$

Where C_x is the concentration of defects x (I or V) and C_x^* is the equilibrium concentration of defect x (I or V). This permits a super-saturation of *interstitials* together with an under-saturation of *vacancies*.

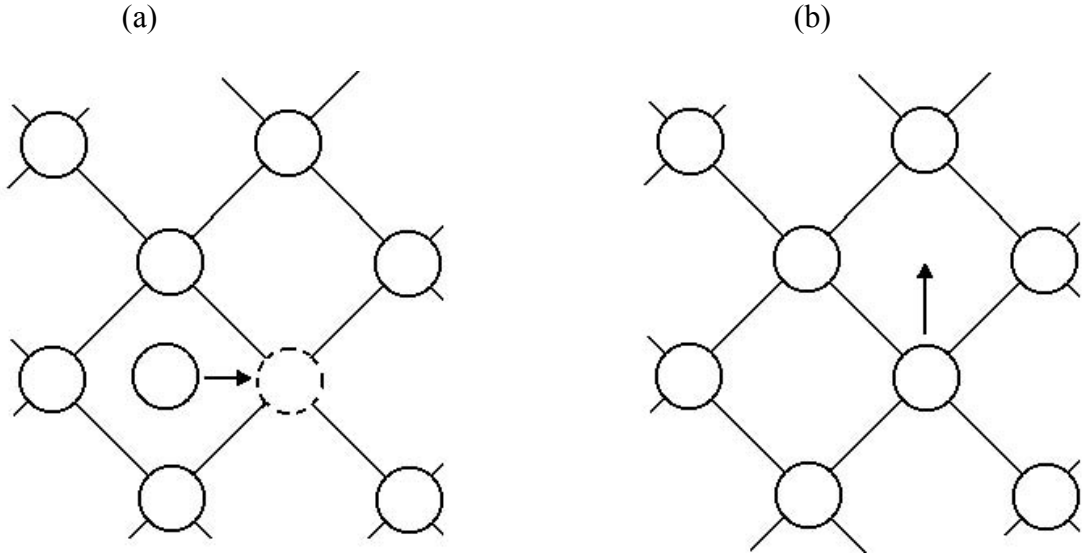

Figure 4.2 Schematic diagram showing: (a) Bulk process $I + V \Rightarrow 0$, (b) Frenkel process $0 \Rightarrow I+V$

The other possibility is an *interstitial* created when silicon atom at the surface moves into the bulk and a *vacancy* formed due to substitutional silicon atom moving to the surface. When silicon crystal is heated, point defects flow into the bulk and the inverse of surface creation process will occurs. The net flux J_x into silicon wafer for point defect is given by equation (4.5) :

$$J_x = \sigma_x (C_x - C_x^*) \tag{4.5}$$

Where σ_x is the recombination velocity for defect x is I or V.

Point defects can also be created by chemical reactions at the silicon surface, for example, thermal oxidation, silicidation and thermal nitridation etc. Another source of point defects is the precipitation of the impurity which occurs when the solubility of an impurity is exceeded in silicon, precipitation of the impurity will occur. There are two with which the precipitation process can affect point defect concentrations. First, there will be a change in the volume due to the formation of a precipitate; for example, when O dissolves largely in the interstitial state O_i, precipitate of SiO_2 will form and it is roughly twice the volume of the pure silicon. Second, if we have *AX* defects, which is responsible for migration of the dopant atoms to and from the precipitates. An example of that will be if we have P*I* defect, it could diffuse to a SiP precipitate and release *I* defect as the P atom stick together with the precipitate [FAHE89]. Dislocation could be considered as a source and a sink of point defects, it forms in regions of the crystal that have few or more atoms per unit volume. As modern techniques are used to grow silicon materials, the dislocation density is so small and usually not considered to be important sources or sinks of point defects [RAFF96, LAMP99]. In addition, point defects can also combine into aggregates [MICH97]. Thus the *free* point defects available for diffusion are limited [DABR00].

It should be noted that there are not only impurity clusters but also vacancy clusters especially after ion implantation [CHAK01].

Ion implantation is a major source of point defects which can severely damage the silicon lattice. The amount of generated defects depends on the implantation energy as well as the dosage. Monte Carlo simulation [HOBL88] and simple models such as *plus-one* ("+1") model [GILE91] can predict the number of point defects generated. The idea of "+1" model is that implantation creates equal numbers of *interstitials* and *vacancies* (*Frenkel* pairs), and one extra *interstitial* for every implanted ion.

4.2. Basic Atomic Level Diffusion Mechanisms

When the dopants introduced into silicon lattice, the impurity concentration gradient causes the diffusion process. In the simplest case, 1-dimensional diffusion which can be easily described by the continuum theory using *Fick*'s diffusion laws (4.6):

$$\frac{\partial}{\partial t}C(x,t) = -\frac{\partial}{\partial x}J(x,t)$$
$$J(x,t) = -D\frac{\partial}{\partial t}C(x,t) \qquad (4.6)$$

Where C is the concentration of the species, J denotes the diffusion flux of the particles, and D is the diffusivity or the diffusion coefficient. These equations are phenomenological, which gives no information about the diffusion at the atomic level. In these equations, the diffusion coefficient is usually calculated from the measurements [SHA75, FAI81]. Random walk analysis and the atomic jump model [JAI75] can also be used to calculate the diffusion coefficient. However, when impurities are implanted into silicon, Fick's laws are not accurate enough to

explain the complex diffusion behavior such as Transit Enhanced Diffusion (TED) and oxidation enhanced diffusion, etc.

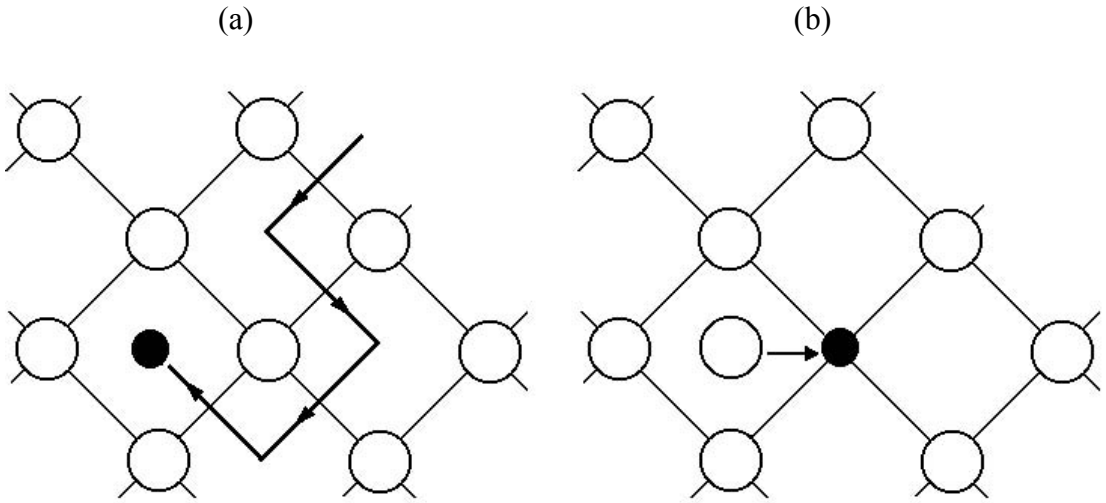

Figure 4.3. Schematic diagram showing direct mechanisms: (a) represents interstitial mechanism and (b) represents kick-out mechanism.

There are different schemes of categories of diffusion mechanisms so it is necessary to focus on the diffusion at atomic level. There are three mechanisms suggested for atomic diffusion [PUCH96]: *Direct* mechanism, *vacancy* mechanism and *interstitial* mechanism. Fahey et al. [FAHE89] used a further popular system: *interstitial* mechanism, *vacancy* mechanism and *interstitialcy* mechanism.

Direct mechanism is shown in Fig. (4.3). The impurities that have small ionic radius can move directly from one interstitial site to another as shown in Fig. 4.3(a). Some authors call it *interstitial* mechanism [PUCH96]. Example for elements that can diffuse with this mechanism are Group-*I* such as H and Group-*VIII* such as Fe, Ni, and Co, etc; therefore these elements are

fast diffusers. When an interstitial atom kicks the atom at substitutional site, diffusion happens as shown in Fig. 4.3(b), which is called *kick-out* mechanism:

$$A_s + I \Leftrightarrow A_i \tag{4.7}$$

The interstitials can be silicon self-interstitials or impurity interstitials.

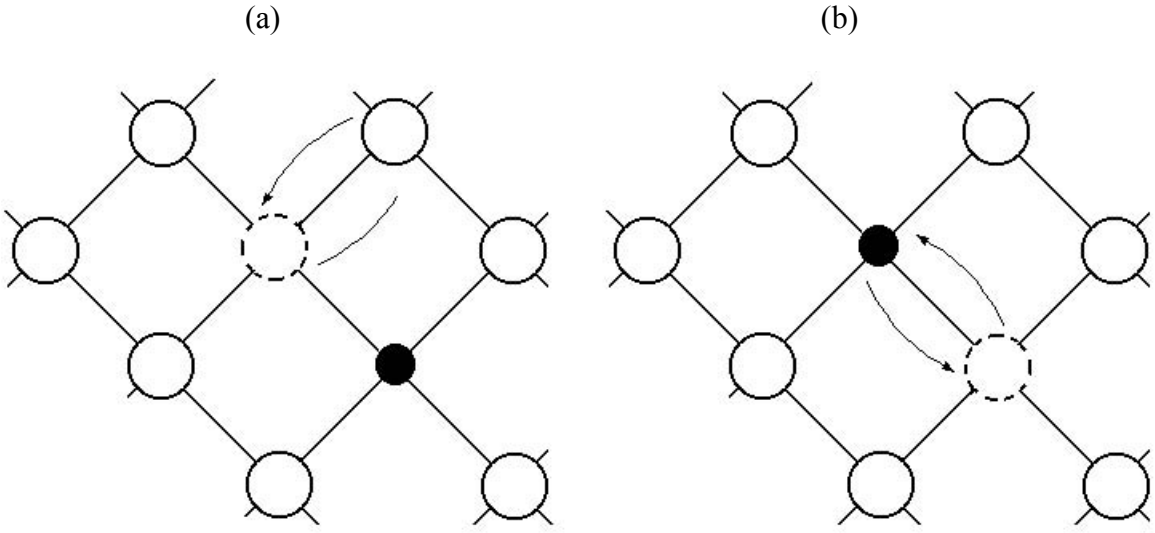

Figure 4.4 Schematic diagram showing vacancy mechanisms: (a) represents Si atom diffusion, (b) represents dopant diffusion

If the atoms move via adjacent vacant lattice sites (Fig. 4.4), the mechanism is called vacancy mechanism.

$$A + V \Leftrightarrow AV \tag{4.8}$$

The diffuser can be host as in figure 4.4 (a) or impurity as in figure 4.4 (b). In the silicon lattice (diamond structure), the vacancy must diffuse to at least a third-nearest neighbor to complete one diffusion step [FAHE89]. In Fig. (4.5) the *interstitialcy* mechanism is shown as

$$A + I \Leftrightarrow AI \qquad (4.9)$$

The interstitialcy can be silicon atom (Fig.4.5 (a)) or impurity atom (Fig.4.5 (b)). The reactions are also called *kick-out* process. Different from the kick-out process of *interstitial* mechanism, the kick-out reactions of *interstitialcy* mechanism happen between substitutional/interstitialcy atoms instead of between substitutional/interstitial atoms.

(a) (b)

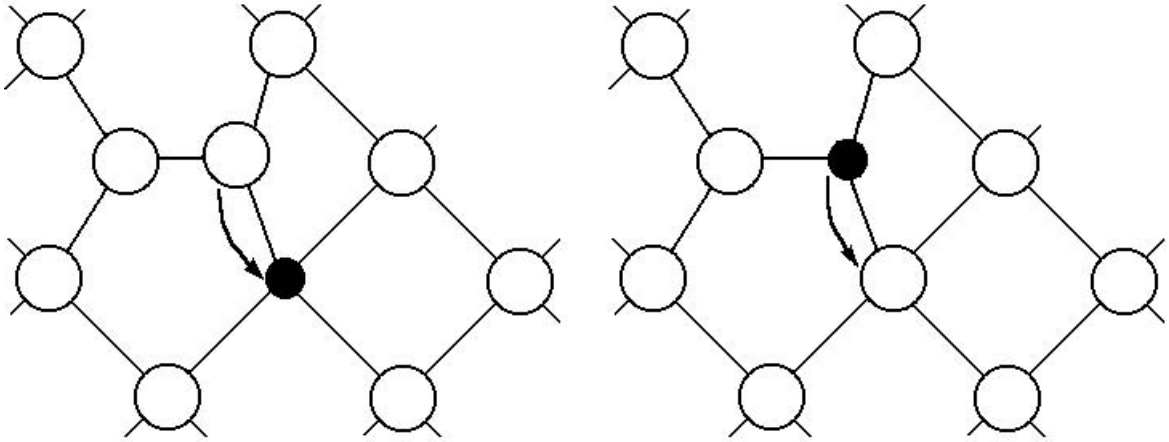

Figure 4.5. Schematic diagram showing interstitialcy mechanism; (a, b) dopant diffuse via a substitutional-interstitialcy interchange

4.3. Diffusion in Poly-silicon

Recently, more attention has been directed to the use of poly-silicon in modern IC fabrication because of the important applications of it in microelectronics such as gate electrodes, thin film transistors and solar cells [RATH03] so the surface topography and the morphology of poly-silicon layer can strongly influence the performance of thin-film layered device structures.

Thermal treatment is important in the morphological structure of poly-silicon but this thermal treatment of is hard to control with respect to reproducibility and reliability [HTTP].

4.4. Impurities Diffusion in Poly-silicon

The diffusion mechanism of dopant during annealing in poly-silicon is very complicated which makes it an area of interest for many researchers [HANE93, MATS93 and JONE90]. From experimental data, poly-silicon shows extraordinary high diffusivity for dopants. Diffusion within poly-silicon involves four major mechanism; fast diffusion in grain boundaries, grain interior diffusion, segregation between grain interior and grain boundaries, grain boundary motion, which allow the dopants to diffuse even long distances within the poly-silicon material in short time. To get a clear picture for dopant/grain boundary system we will have a closer look onto the crystal structure of a grain bulk/grain boundary arrangement. Two poly-silicon grains separated by a grain boundary and having tetrahedral bonding system are shown in fig. (4.6). In this figure, we see that the numbers of bonds going from one grain to the other is reduced at the interface; therefore this boundary area is good for dopant fast diffusion.

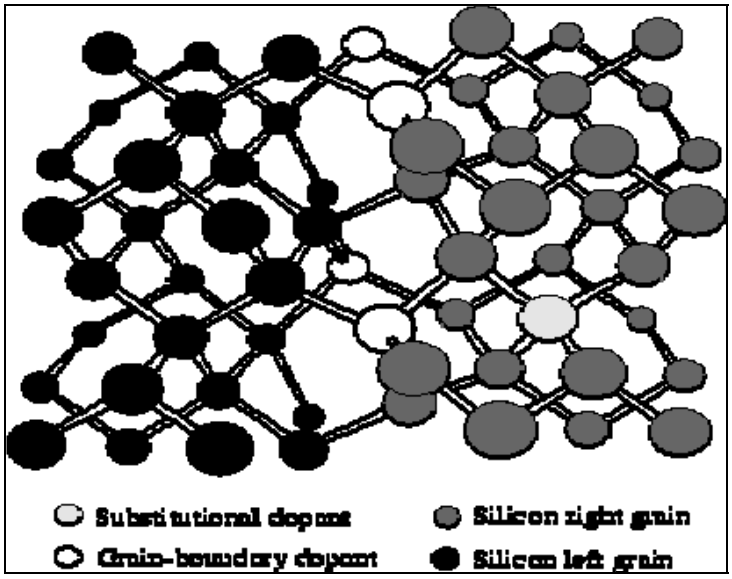

Figure 4.6 shows three-dimensional perspective drawing of a grain/grain boundary network in poly-silicon. [HTTP]

As shown in fig. (4.6), dopants show high probability to segregate into the grain boundary. Dopants can segregate into the grain boundary area if there is enough space in the grain boundary and are close enough. The segregation mechanism at the grain boundary can be illustrated by emission or catching dopants. The rate of trapping and emission of dopants depends on the free states and the number of dopants in the grain boundary area.

The third mechanism is the grain boundary motion which is related to the grain growth. The grain boundaries are moving and so do the dopants in the grain boundary area due to the grain growth. According to these movements there will be a net dopant transport.

For the grain interior diffusion, the crystal structure of the poly-silicon grain bulk region shows a normal silicon lattice. Therefore the diffusion of the dopants within the grain interior regions will be treated as normal bulk diffusion in silicon.

4.5. Grain Boundary Diffusion versus Volume Diffusion

Grain boundary plays an essential role in the diffusion in poly-silicon as mentioned previously. It is the process of atomic transport along the grain boundary in crystalline materials [KAUR95]. Grain boundaries are highly disordered regions of finite thickness between two ordered crystals. This disordered region provides a slightly open medium for atomic transport. As a result, grain boundary diffusion is typically several orders of magnitude faster than diffusion through the crystalline lattice. Grain boundary diffusion and volume diffusion are described by Fick's laws. The first one states that the diffusion flux J is proportional to the concentration gradient in the direction of diffusion as shown in equation (4.10).

$$J = -D\nabla c \tag{4.10}$$

Where D is the diffusion coefficient and (∇c) is the concentration gradient. The negative sign indicates that the flow of the dopant is in the decreasing concentration direction. The diffusion coefficient in this form depends on concentration, time, and position. Fick's second law relates the rate of change of the concentration to the concentration gradient as in equation (4.11)

$$\frac{\partial c}{\partial t} = D\nabla^2 c \tag{4.11}$$

Fick's laws are valid just in the case when diffusion is driven by a concentration gradient. The solution to equation (4.11) is given by equation (4.12)

$$c(z,t) = c_0 erfc(\frac{z}{2\sqrt{Dt}}) \tag{4.12}$$

From the solution we can see that the concentration varies parabolically with depth. D can be determined from fitting equation (4.12) to the concentration distribution determined from

experiment. Moreover, the diffusion coefficient in equation (4.12), exhibits an Arrhenius type relationship according to equation (4.13)

$$D = D_0 \exp(\frac{-Q}{kT}) \tag{4.13}$$

where D_o is the temperature independent pre-exponential factor, Q is activation energy for the diffusion process, *k* is Boltezman constant and T is the absolute temperature. All these equations describe volume diffusion.

In order to see the differences between polycrystalline and monocrystalline diffusion rates, Fisher [FISH51] resolved the problem for grain boundary diffusion. He implicated that the grain boundary was a uniform rectangular slab with width δ where fast diffusion can occur. Additionally, leakage of the diffusing species may also occur laterally from the grain boundary slab into the crystal from areas in which there is no direct contribution from volume diffusion. Fisher's model showed that the logarithm of the average concentration varied linearly with the depth into the material. He developed an approximate solution to the problem of grain boundary diffusion. A typical diffusion profile schematic diagram is shown in fig. (4.7). Others like Whipple [WHIP54] provided an exact solution for grain boundary diffusion using Fourier-Laplace transforms, but it is not working well for experimental data. LeClaire [LECL63] used Whipple's solution and developed it to provide very good results within a particular range of parameters and it is known as Whipple-LeClaire solution, for more details see [WHIP54, LECL63].

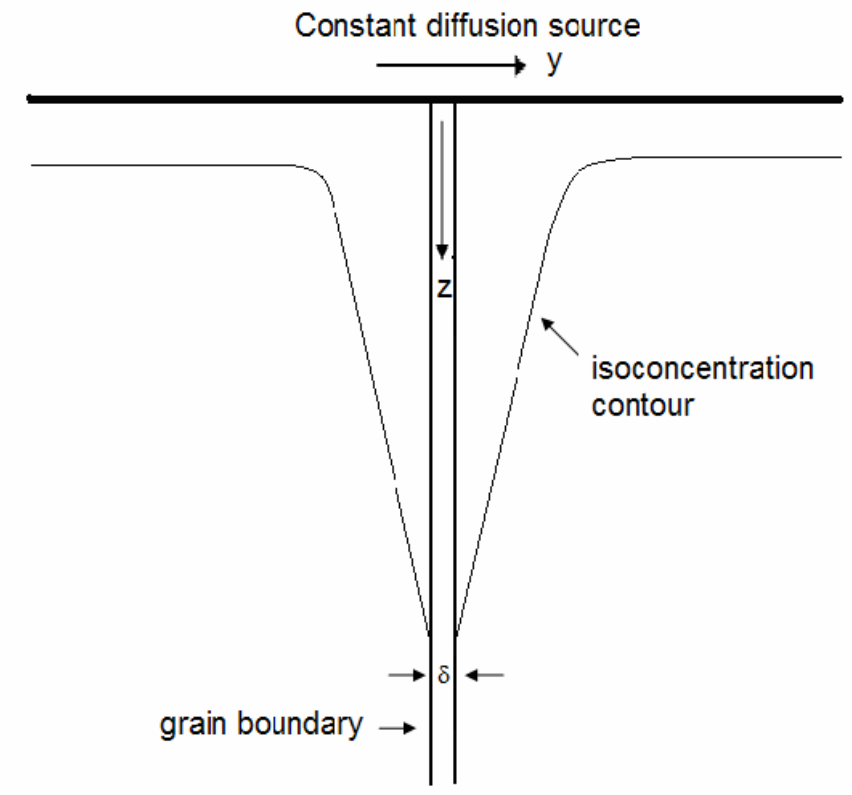

Figure 4.7. Schematic diagram of a typical diffusion profile in agreement with the fisher model. [FISH51]

4.6. Diffusion in Silicides

There was and always be a big concern about the impurity diffusion into silicides mainly diffusion of Si dopants. The umber of silicides such as WSi_2, $TiSi_2$, $CoSi_2$, $MoSi_2$ and $TaSi_2$ that have been studied in that case is limited and subjective by their technological application. Self and impurity diffusion data have been reviewed [GAS95, GAS98]. The demand to study the characteristics and the properties of transition metal silicides come from their uses in integrated circuit technology. In this section we will give a quick overview on diffusion in silicides. As mentioned earlier, diffusion is based on Fick's laws [FICK55] where the diffusion flux is proportional to the concentration gradient. This is fine when concentration is the only dynamic

force but the diffusion process is more complex. Moreover, the diffusion coefficients are realized from mass transport (concentration profiles) and mass transport will depend on all the diffusion paths including dislocation (d), surfaces (s) and grain boundaries (gb). Then the diffusion flux is a combination of the diffusion flux through these different defects [MANN68, PHIL91]. The simplest form is shown in equation (4.14)

$$J_{tot} = (1 - (\alpha_d + \alpha_{gb} + \alpha_s) J_V + \alpha_d J_d + \alpha_{gb} J_{gb} + \alpha_s J_S) \tag{4.14}$$

Where α is the number of defect sites divided by the total number of sites.

As we mentioned before, the redistribution of unwanted elements may have unwanted consequence on the electrical characteristics of the device. On the other hand, distribution of dopants from the silicide layer into Si may be used usefully in order to generate shallow junctions. The diffusion mechanism is complex because there are several mechanisms such as volume and grain boundary diffusion, solubility limits, dopant distribution and segregation at the interfaces and grain boundary. Most of the experimental data are obtained by classical analysis using SIMS [GAS86]. Others provided diffusion information by electrical measurements of lateral diffusion of dopant in silicides lines [CHU93]. The characteristics of thermal modifications of dopants implanted in silicide films are: 1) an accumulation at the silicide/silicon interface [THOM88], 2) a smoothening around the implantation peak, and 3) a concentration increase in the center of the layer. The increases in the center layer in addition to the accumulation at the silicide/Si are the result of rapid grain boundary and interface diffusion while the changes around the implantation peak are due to the volume diffusion.

4.7. References

[BLÖC93] P. E. Blöchl, E. Smargiassi, R. Car, D. B. Laks, W. Andreoni and S. T. Pantelides, Phys. Rev. Lett. **70**, 2435 (1993).

[BRAC91] H. Bracht, N. A. Stolwijik, H. Mehrer and I .Yonenaga, Appl. Phys. Lett. **59**, 3559 (1991).

[BUNE00] M. M. Bunea, S. T. Dunham, Phys. Rev. B **61**, 2397 (2000).

[CHAK01] S. Chakravarthi, S. T. Dunham, J. Appl. Phys. **89**, 4758 (2001).

[CHAS97] E. Chason, S. T. Picraux, J. M. Poate, J. O. Borland, M. I. Current, T. Diaz de la Rubia, D. J. Eaglesham, O. W. Holland, M. E. Law, C. W. Magee, J. W. Mayer, J. Melngailis and A. F. Tasch, J. Appl. Phys. **81**, 6513 (1997).

[CHU93] C. L. Chu, K. C. Saraswat and S. S. Wong, IEEE Transactions on electron devices **39**, 2333 (1993).

[CLAR97] S. J. Clark and G. J. Ackland, Phys. Rev. B **56**, 47 (1997).

[DABR00] J. Dabrowski, Solid State Phenomena **71**, 23 (2000).

[DABR99] J. Dabrowski, H. -J. Mussig, M. Duane, S. T. Dunham, R. Goossens and H. -H. Vuong, Advances in Solid State Physics **38**, 565 (1999).

[DUNH92] S. T. Dunham, J. Appl. Phys. **71**, 685 (1992).

[EAGL94] D. J. Eaglesham, P. A. Stolk, H.-J. Gossmann and J. M. Poate, Appl. Phys. Lett. **65**, 2305 (1994).

[FAHE89] P. M. Fahey, P. B. Griffin and J. D. Plummer, Reviews of Modern Physics **61**, 289 (1989).

[FAI81] R. B. Fair, In: Impurity Doping Processes in Silicon. North Holland, Amsterdam, 315 (1981).

[FICK55] A. Fick, Philos. Mag. **10**, 30 (1855).

[FISH51] J. C. Fisher, J. Appl. Phys. **22**, 74 (1951).

[GAS86] P. Gas, V. Deline, F. M. d'Heurle, A. Hichel and G. Scilla, J. Appl. Phys. **60,** 1634 (1986).

[GAS95] P. Gas and F. M. d'Heurle,: *properties of Metal silicides*, *edited* by K. Maex and M. van Rossum, IEE, London, (1995).P.279.

[GAS98] P. Gas and F. M. d'Heurle, in Landolt-Bornstien, Diffusion in Semiconductors and Non-Metallic Solids, *edited* by D. L. Beke (Springer Verlag, Berlin, 1998).

[GILE91] M. D. Giles, J. Electrochem. Soc. **138**, 1160 (1991).

[GOSS93] H. J. Gossmann, C. S. Rafferty, H. S. Luftman, F. C. Unterwald, T. Boone and J. M. Poate, Appl. Phys. Lett. **63**, 639 (1993).

[HANE93] M. Hane and S. Hasegawa, In Poly-Si, Grain-Growth, 52 (1993).

[HOBL88] G. Hobler and S. Selberherr, IEEE Transactions on Computer-Aided Design **7**, 174 (1988).

[HTTP] http://www.iue.tuwien.ac.at/phd/puchner/node34.html

[HU73] S. M. Hu, Diffusion in Silicon and Germanium, in Atomic Diffusion in Semiconductors edited by D. Shaw, Plenum Press (1973).

[JAI75] R. K. Jain and R. J. Van Overstraeten, J. Electrochem. Soc. **122**, 552 (1975).

[JARA96] M. Jaraiz, G. H. Gilmer, J. M. Poate, and T. D. de la Rubia, Appl. Phys. Lett. **67**, 409 (1996).

[JONE88] K. S. Jones, S. Prussin and E. R. Weber, Appl. Phys. A **45**, 1 (1988).

[JONE90] S. K. Jones, Material Research Soc **182**, 129 (1990).

[KAUR95] I. Kaur, Y. Mishin, W. Gust, *Fundamentals of Grain and Interphase Boundary Diffusion*, Wiley, New York, (1995).

[LAMP99] E. Lampin, V. Senez and A. Claverie, J. Appl. Phys. **85**, 8137 (1999).

[LECL63] A. D. LeClaire, British J. Appl. Phys. **14**, 351 (1963).

[LIST98] S. List and H. Ryssel, J. Appl. Phys. **83**, 7585 (1998).

[MANN68] J. R. Manning, *Diffusion kinetics for atoms in crystals* (D. Van Nostrand Company Inc., Princeton, 1968).

[MATS93] M. A. Matsuoka and S. T. Dunham, Dopant Diffusion in Polysilicon. In Proceedings: Third International Symp. On process Physics and Modeling in Semiconductor Technology, Hawaii, Honolulu, (1993), Ed. By G. R. Srinivasan, pp. 88.

[MAYE70] J. W. Mayer, L. Erikson and J. A. Davis, *Ion Implantation in Semiconductors-Silicon and Silicon and Germanium*, Academic Press (1970).

[MICH97] J. Michel, L. V. C. Assali, M. T. Morse and L. C. Kimerling, *Erbium in Silicon, in Semiconductors and Semimetals Vol.49 edited* by David J. Lockwood, Academic Press (1997).

[MYER00] S. M. Myers, M. Seibt and Schröter, J. Appl. Phys. **88**, 3795 (2000).

[PHIL91] J. Philibert, *Atom Movements-Diffusion and mass Transport in Solids* (Les Editions de Physique, Paris, 1991).

[RAFF96] C. S. Rafferty, G. H. Gilmer, M. Jaraiz, D. Eaglesham and H. J. Gossmann, Appl. Phys. Lett. **68**, 2395 (1996).

[RATH03] J. K. Rath, Solar Energy Materials & Solar Cells **76**, 431 (2003).

[SEEG68] A. Seeger and K. P. Chik, Phys. Stat. Sol. **29**, 455 (1968).

[SHA75] D. Shaw, Phys. Stat. Sol. B **72**, 11 (1975) .

[SWAL73] R. A. Swalin, The Calculation of Diffusion Coefficients in Semiconductors, in Atomic Diffusion in Semiconductors edited by D. Shaw, Plenum Press (1973).

[THOM88] O. Thomas, P. Gas, A. Charai, F. K. LeGouses, A. Michel, G. Scilla and F. M. d'Heurle, J. Appl. Phys. **64**, 2973 (1988).

[WHIP54] R. T. Whipple, Philosophical Magazine **45**, 1225 (1954).

[WOLF00] S.Wolf and R. N. Tauber, *silicon processing for the VLSI Era*, Volume 1- Process Technology, Second Edition. Lattice Press (2000).

CHAPTER 5
DIFFUSION OF TRANSITION METALS SUCH AS CR AND V INTO (100) CRYSTALLINE SILICON SUBSTRATES

5.1. Introduction:

Transition metal impurities diffusion in silicon is an important topic in devices processing, due to the fact that transition metals are fast diffusers in crystalline silicon and major contaminants in silicon processing. There were many investigations [GRAF00] on the behavior of transition metal impurities in silicon. Transition metals have damaging effects on performance, reliability and the yield of semiconductor devices. Transition metal contaminations could be found anywhere during the fabrication of silicon devices [GRAF00], for example during the deposition, cleaning, crystal growth, plasma etching, annealing, and ion implantation. Major 3d transition metal contaminants such as Fe [ISTR00, ISTR99], Ni [JONE95, SPIT89], and Cu [NAKA00, ISTR98] are common because of the use of stainless steel in the integrated circuit (IC) fabrication process. Kikoin et al. [KIKO94] reported that the transition metal contaminates in silicon, even at very low concentration, can harmfully influence the device performance. As the charge carrier generation/recombination centers or electrical shorts, transition metal impurities will have significant effect on the properties of silicon. This is why there were extensive study on transition metal contaminates in silicon [WEBE83, SEIB88, JOLY98 and GRAF00]. In this section we will present our study on the distribution behavior of low dosages of Cr and V dopants in silicon.

5.2. Experiment

Chromium and Vanadium ions were introduced into Silicon (100) single crystalline substrates by ion implantation at room temperature. The implantation was carried out at Implant Sciences Corporation. The implantation energy is 200 keV; the doses are 10^{13} cm^{-2} and 10^{12} cm^{-2}. Thermal annealing were carried out for the implanted samples at temperatures from 300°C to 1000°C, for 30 minutes each, and at temperatures 450°C and 550°C for different time intervals (5, 15, 30, 60, 120, 240 minutes). The annealing processes were held at Lindberg furnace with a long quartz tube as shown in fig. 5.1. Once the desired temperature was reached, the quartz tube with the samples was placed into the center of the furnace. The annealing temperature was accurately controlled (nominally ± 1°C). A constant flow of high purity (99.999 %) Ar gas was maintained through the quartz tube during the annealing process. After completion of the annealing process, the quartz tube was pulled out and moved away from the center of the furnace and the samples were cooled to room temperature in argon atmosphere.

Secondary Ion Mass Spectrometry (SIMS) was used to obtain depth profiles of the impurities. SIMS characterization was carried out at the UCF/Agere Materials Characterization Facility with a CAMECA IMS-3f using 100 nA or 150 nA (measured using improved Faraday cup and checked by sputtering rate and primary current comparison with a CAMECA IMS-6f) O_2^+ primary ion beam at a source potential of 10 kV, an impact energy 5.5 keV and impact angle 40° from normal. The focused primary beam of oxygen ions was raster over a 200 x 200 μm^2 or 250 x 250 μm^2 areas, with detection of ions from an area of 60 μm diameters at the center of the raster.

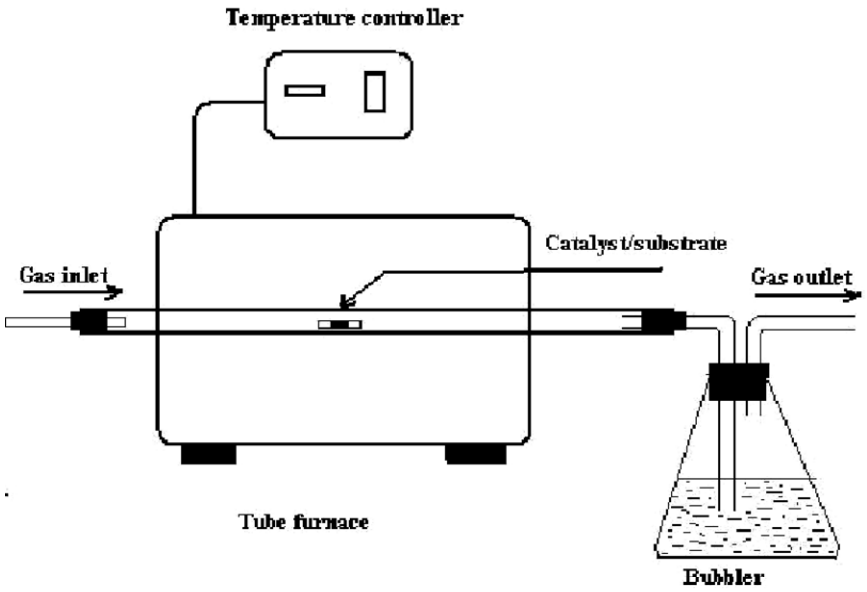

Figure 5.1 Schematic diagram howing Lindberg furnace with a long quartz tube.

The sputtering rate was determined to be 0.6nm/s. The depth scale was established for each profile by measuring the crater depth with a stylus profilometer (Sloan Dektak IIA). The concentration was calibrated with the implantation dosages of the as-implanted sample and the measured sputtering rate.

5.3. Chromium Implanted into Silicon

5.3.1. Introduction

Despite the work done over the last several decades; there are many gaps in the diffusion data, even for materials such as silicon and silicon dioxides [FISH99, FAIR88, KONU91 and SHAC93]. Ion implantation used to introduce dopant atoms into silicon substrates. Over the years, ion implant has replaced thermal diffusion because of its many advantages. As mentioned

in chapter 2, the greatest advantage is its precise control for introducing impurity atoms into the substrate. Annealing is used to heal the damage in the crystal lattice caused by ion implantation and to activate the dopants [JONE88, CHAS97].

Chromium ions can reduce the carrier lifetime and corrupt the device performance. So it is important to study the diffusion mechanism of Cr, to control the redistribution of these impurities in silicon devices. There were few publications on diffusion of Chromium implanted into silicon other than the work of Wilson et al. [WILS80, WILS81 and JUN-T83], and work done by Francois. et al.[FRAN01]. There is still a lack of detailed information about the role of damage during the annealing process of Cr implanted into Si.

Recently, diffusion profiles of Chromium with dosages ranging from 10^{14} to 10^{15} cm^{-2} have been studied [ZHAN01] at temperatures from 300°C to 1000°C. The high dosage results [FRAN01, ZHAN01] were explained by the amorphorization of the silicon substrate and the subsequent solid phase epitaxial growth of the amorphous layer. As the implantation dosages drop below the amorphorization threshold, no amorphous layer will be formed. The diffusion profiles after thermal anneals will be dominated by the interactions between the implanted dopant ions and the defects created by ion implantation.

At low dosage, the diffusion profiles are very complicated, indicating a complex behavior. In order to better understand the complexity of this behavior, we extended the study of diffusion of Cr at low dosages 10^{12} cm^{-2} and 10^{13} cm^{-2} in silicon using ion implantation.

The redistribution of impurities profiles are characterized by Secondary Ion Mass Spectrometry (SIMS), which is based on the mass spectrometric analysis of ions, which are generated by the interaction of a primary ion beam (keV range) with the sample to be analyzed as mentioned in more details in chapter 3. Because of its high sensitivity and depth resolution, SIMS is widely used for analysis of trace elements in solid materials, especially semiconductors [FELD86, SCHR99] but mobility of species during analysis must be taken into account, especially for alkali elements [HUGG72, MAGE78].

5.3.2. Results and Discussion

Chromium ions with low dosages (10^{13} cm^{-2} and 10^{12} cm^{-2}) are introduced into silicon with ion energy of 200 keV. These dosages are below the threshold value to produce an amorphous layer.

Starting with Fig. 5.2(a), depth profiles of $1x10^{13}$ cm^{-2} Cr implanted into silicon are presented. For 300°C annealing, Cr impurities started at to diffuse slightly into the substrate. After annealing at 500°C a contraction behavior appeared, this is suggested to be a result of Cr clustering reactions. The depth profile of 700°C annealed sample showed a peak at the implantation projection range R_p. It is not very clear whether this peak is the result of the residues of Cr clusters or it is caused by complex defect near the projection range of the ion implantation. At 900°C, that defect dissolved and most of Cr atoms are in the top 0.1 μm and a large part of the implanted Cr ions were evaporated during annealing [ZHAN01]. Annealing at 1000°C, the diffusion profile is slightly different than the diffusion behavior of the Cr ions annealed at 900°C. It shows a slightly diffusion more in the sample. At this moment, we do not

have a satisfactory explanation for this phenomenon. We speculate that to the formation of oxide layer from minute impurities in Ar gas.

In fig. 5.2(b), SIMS profiles of Cr ions $1x10^{12}$ cm^{-2}, as-implanted and annealed samples, are shown. The profiles for the 300°C annealed sample is the same as that of the as-implanted sample. At 500°C anneal, the Cr redistribution starts. The Cr ions diffuse deeper into the silicon substrate. At 700°C most of the Cr impurities are driven to the surface, this can be due to the low dosage of Cr, which is not enough to form any kind of defect. At 900°C and 1000°C, Cr impurities started to diffuse more into Si substrate. It may be due to the dissociation of the Cr clustering reactions at higher temperatures or due to oxidation enhanced diffusion (OED). This is a complex behavior and it is not easy to explain.

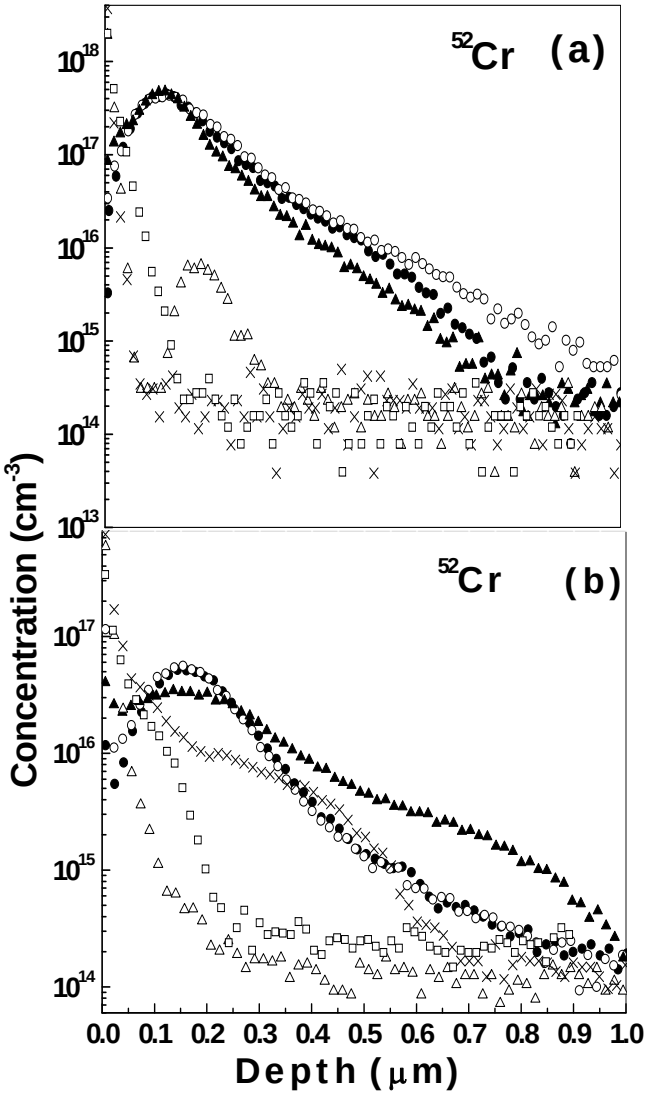

Figure 5.2 SIMS depth profiles (a) 10^{13} and (b) 10^{12} of ^{52}Cr cm^{-2} implanted with 200 keV into Si and annealed for 30 minutes in Ar gas (● As-implanted, ○ 300°C, ▲500°C, Δ 700°C, × 900°C, □ 1000°C).

For better understanding of the complex behavior of Cr ions in silicon, we studied the diffusion behavior of these ions at 450°C for different time intervals. Fig. 5.3(a) shows SIMS profiles of Cr $1x10^{13}$ cm^{-2} of as-implanted and 450°C annealed samples. For 1-hour annealing sample, depth

profile showed a contraction behavior. As the annealing time increases to 2 and 4 hours the concentration depth profiles showed almost no diffusion of the Cr impurities in Si substrate; in this situation we can say that at 1 hour annealing the impurity ions formed clusters which act as a trap for the other ions and kept them from diffusing in silicon. As the time of annealing increases to 2 and 4 hours, the clustering reaction might start to slow down and the impurity ions diffuse slightly more in silicon. However, the general observation is that all the samples showed shrinking behavior than the as-implanted sample.

SIMS profiles of the 200 keV Cr, $1x10^{12}$ cm^{-2} implanted and annealed samples at 450°C for different time intervals (1 hr, 2 hrs and 4 hrs) are presented in fig. 5.3(b). The diffusion profiles show almost no changes. At low concentration 10^{12} cm^{-2} the diffusion behavior of Cr ions doesn't show almost any diffusion. This is due to "very small diffusivity" of low concentration Cr ions in silicon substrate.

There is anomalous behavior was seen many times in the diffusion profiles for low concentrations Cr ions. First the impurity ions started to show in-diffusion mechanism and then out-diffusion mechanism and after that started to show in-diffusion mechanism again. To elucidate our SIMS observation of Cr ions profile after annealing; we extended our study to annealing temperature of 550°C for different time intervals. In fig. 5.4(a), SIMS profiles of the Cr ions, $1x10^{13}$ cm^{-2} for as-implanted and for annealed samples are illustrated. This time, we raised the temperature to 550°C and decreased the annealing time. Unfortunately, the depth profiles show even more complex behaviors. The concentration profile of Cr ions shows a contraction behavior at 5 minutes annealing sample, and even more for 15 and for 30 minutes

annealing samples. However, the profile after 60 minutes annealing at 550°C seems to be the same as that annealed at 550°C for 15 minutes. We decreased the implanted dose of the Cr ions to 10^{12} cm^{-2}. The depth profiles for as-implanted and 550°C annealed samples is presented in fig. 5.4(b) . The diffusion profiles show strange behavior that we didn't observe before in any of the samples and it is not easy to explain and more work needed.

According to what obtained from SIMS depth profiles, the diffusivity of some low dosages Cr was calculated and compared with some previous [SADO91, WEBE83] The diffusion coefficient of [SADO91] Cr in Si has been determined from these concentration profiles using equation (5.1)

$$C(x) = C_O \exp\left(\frac{-(x - x_m)^2}{2(\sigma^2 + 2Dt)}\right) \qquad (5.1)$$

Where x_m is the peak position and σ is the halfwidth of the as-implanted concentration depth profile, D and t are the diffusion coefficient and the diffusion time. We found that the diffusivity of $1x10^{12}$ cm^{-2} Cr ions annealed at 450°C is $8.30x\ 10^{-16}$ cm^2/s. The calculated diffusivity in our work is low compared to some previous work, D is ~ $1x10^{-14}$ cm^2/s [WEBE83, SADO91].

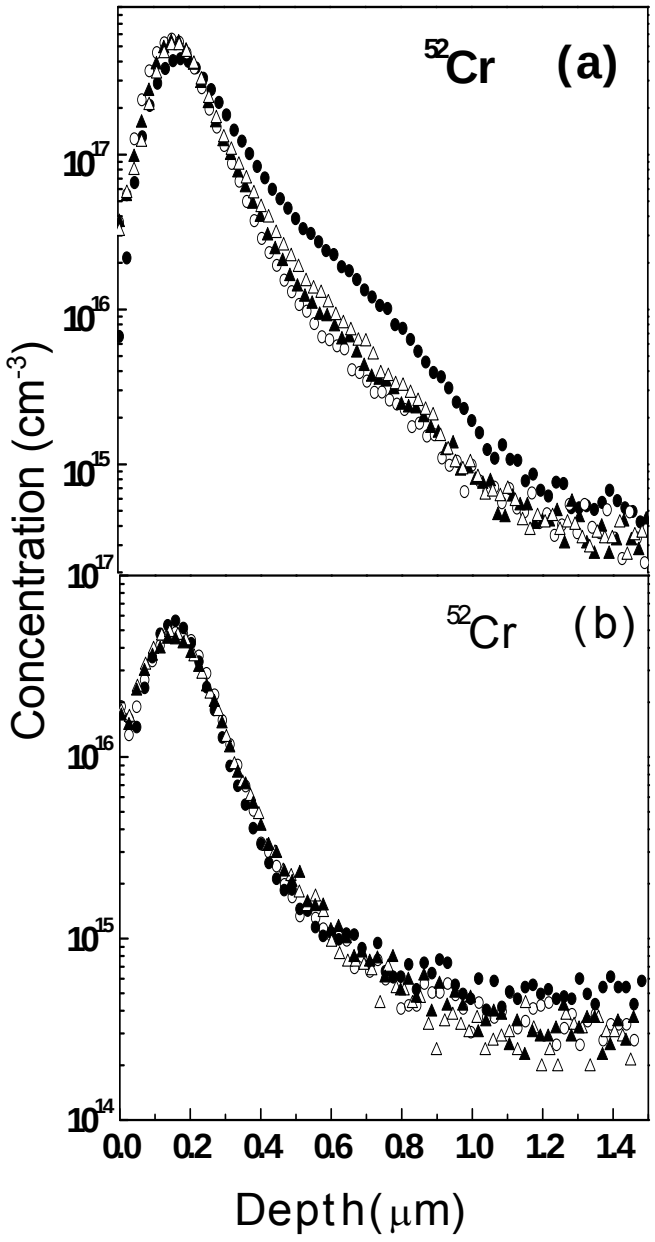

Figure 5.3 SIMS depth profiles (a) 10^{13} and (b) 10^{12} of ^{52}Cr cm^{-2} implanted with 200 keV into Si and annealed at 450°C for different times in Ar gas (● As-implanted, ○ 1 hr, ▲ 2 hrs, Δ 4 hrs).

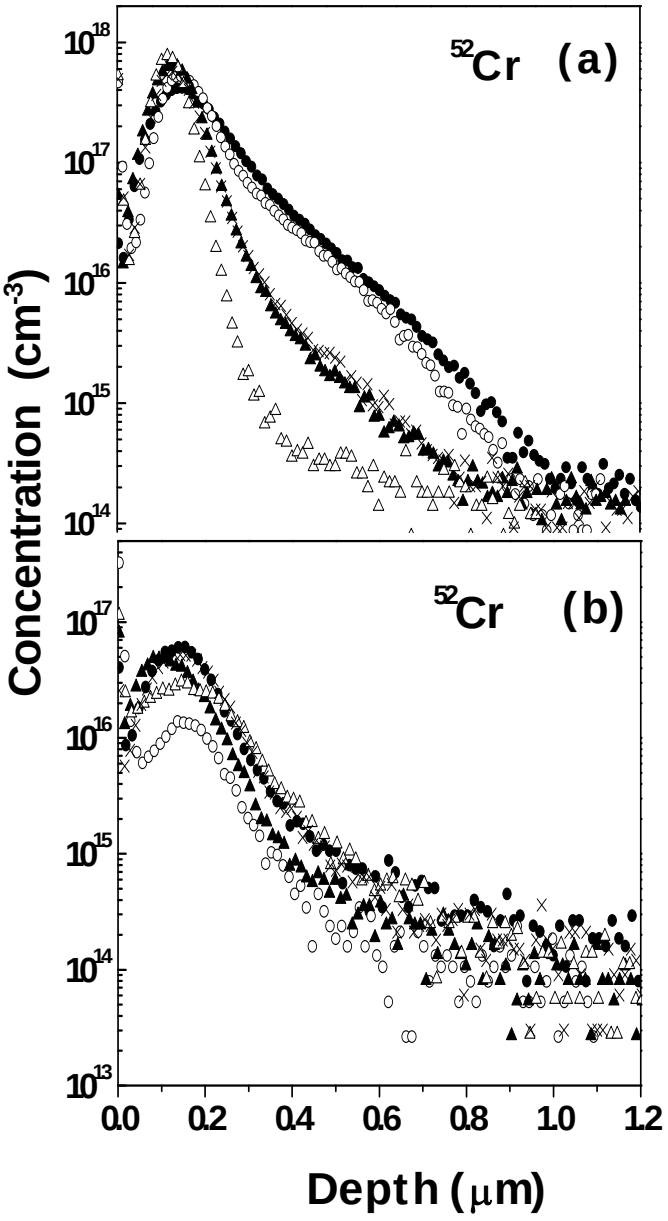

Figure 5.4 SIMS depth profiles (a) 10^{13} and (b) 10^{12} of ^{52}Cr cm^{-2} implanted with 200 keV into Si and annealed at 550°C for different times in Ar gas (● As-implanted, ○ 5 minutes, ▲ 15 minutes, Δ 30 minutes, × 60 minutes).

5.3.3. Summary

The redistribution of low dosage Cr profiles, which are characterized by Secondary Ion Mass Spectrometry (SIMS) were investigated. We found that the diffusion profiles of Cr implanted into silicon are strongly depending on the dosages, the annealing temperature, the annealing time and most of all the defects and the damages caused by ion implantations.

5.4. Diffusion of V into Silicon

5.4.1. Introduction

The 3d transition metals initiate deep levels in the forbidden energy gap in silicon. This makes them technologically important because these deep levels can act as recombination centers or traps which can harshly affect the performance of electronic devices. The transition metals are also interesting from the scientific point of view and have been studied intensively, both experimentally and theoretically. Diffusion processes play a vital role in the device fabrication and understanding of these processing helps making better devices.

There is a big difference in diffusion of the 3d transition metal impurities when compared to each other [GRIE96, GANT91, OHSA90 and XU88]. Vanadium (V) is one of the transition metals that diffuses interstitially in silicon with low diffusion coefficient, which is about three orders of magnitude lower than iron (Fe) at 1000°C [NAKA92]. Kutt et al. [KUTT84] reported that diffusion and redistribution are slower for V than for Cr. More work have been carried out on the diffusion of Cr in GaAs [YU91, BCHE04] and in Si [WILS80, WILS81 and JUN-T83]. But very few diffusion data of Vanadium are available.

In this section, we will focus on the diffusion phenomena of the Vanadium ions implanted into silicon. Ion implantation used to introduce V ions into silicon. The implantation process generates damages and thermal treatment is needed to activate the dopants [JONE88,CHAS97].

Secondary Ion Mass spectrometry (SIMS) is used for characterization of the concentration-depth profiles of V into silicon. These measurements, performed at room temperature for V ions with dosages 10^{13} $cm^{-2}$and 10^{12} cm^{-2}.

5.4.2. Results and Discussion

In this work we will study the behavior of V ions with low dosages 10^{13} cm^{-2} and 10^{12} cm^{-2}. These ions are introduced into (100) silicon substrates with ion energy of 200 keV. Fig. 5.5(a) illustrates SIMS profiles of V ions, $1x10^{13}$ cm^{-2}, for as-implanted and annealed samples for 30 minutes each. For 300°C annealed sample, the impurity concentration-depth profile remained the same as that of the as-implanted one. As the annealing temperature increased to 500°C, V ions started to show more diffusion into the silicon substrate. The annealing behaviors of V atoms at low temperatures 300°C and 500°C were as expected. However, after 700°C annealing the vanadium profile shows contraction. This type of behavior has been observed previously in the diffusion behavior of Cr implanted into silicon. We suspect that, there is a competition between diffusion that causes the broadening of the profile and impurity clustering that causes the contraction of the profile. After 900°C and 1000°C annealing, anomalous peak shifting is observed. The location of the new peaks is near the projection range R_p. It seems that during high temperature annealing, the defects at R_p act as a sink for V ions. Another suggestion could be due

to oxidation during annealing at very high temperature. This may come from the gas we introduced during annealing process or come from the cooling process itself. This peak shift has not been observed in other annealed samples.

In Fig. 5.5(b), the depth profiles of V ions implanted at a dosage of $1.0x10^{12}$ cm^{-2} and annealed samples for 30 minutes at different temperatures are presented. Different from 300°C-annealed V sample with $10^{13}cm^{-2}$ implantation dosage shown in fig. 5.5(a), this sample displayed some diffusion behavior started at 0.3μm. At 500°C, the depth profile showed even faster diffusion than 300°C as expected. After 700°C annealing, the depth profile show contraction and the tail part of the concentration-depth profile changes a little compared to that of the as-implanted sample. It is expected that there are some defects that act as traps for V atoms, also silicon surface attracts the V atoms. At 900°C, the profile showed further contraction of the tail end, and more V atoms started moving to the surface. For the 1000°C-annealed sample, the profile showed a minimum or a dip at 0.1μm below the surface. It is not obvious why, but we can speculate that to surface impurities that attracted V ions at very high temperature.

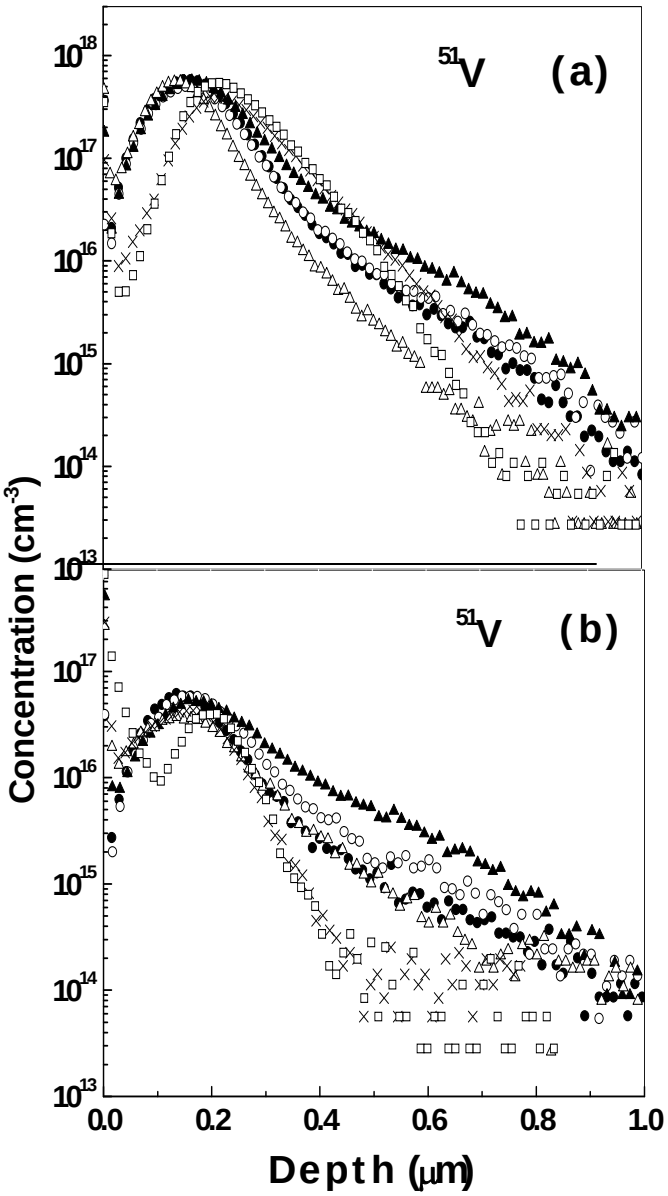

Figure 5.5 SIMS depth profiles (a) 10^{13} and (b) 10^{12} of ^{51}V cm^{-2} implanted with 200 keV into Si and annealed for 30 minutes in Ar gas (● As-implanted, ○ 300°C, ▲500°C, Δ 700°C, × 900°C, □ 1000°C).

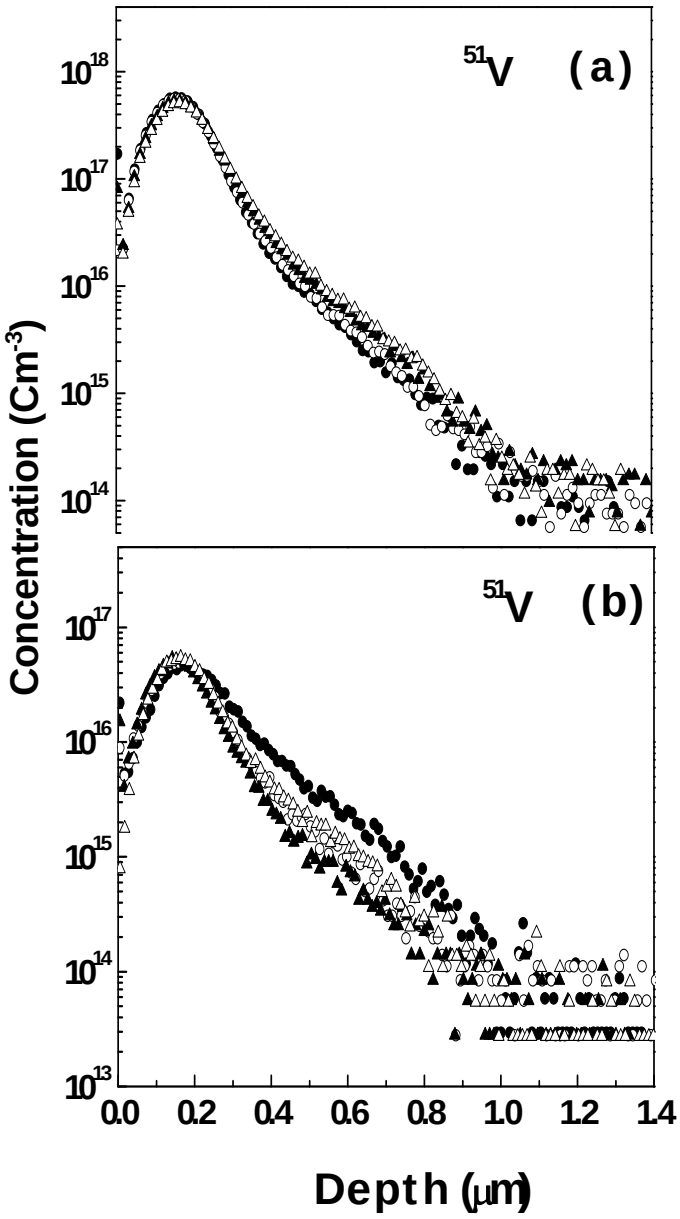

Figure 5.6 SIMS depth profiles (a) 10^{13} and (b) 10^{12} of ^{51}V cm^{-2} implanted with 200 keV into Si and annealed at 450°C for different times in Ar gas (● As-implanted, ○ 1 hrs, ▲ 2 hrs, Δ 4 hrs).

For most of the samples that studied, we noticed a change in the diffusion behavior around 500°C, so to further understand the diffusion behavior of V ions in silicon, we extended our study for annealing at temperatures just below and above 500°C (450°C and 550°C) for different time intervals. Fig. 5.6(a) shows depth profiles of 10^{13} cm^{-2} V ions of the as-implanted and annealed samples at 450°C for 1 hr, 2 hrs and 4 hrs. The diffusion profiles show slightly diffusion of V ions in Si substrate as the annealing time increases. This agreed with Kutt et al. [KUTT84], V ions have slow diffusion and distribution behavior in silicon. SIMS profiles of V ions,10^{12} cm^{-2}, are presented in fig. 5.6(b) for as-implanted and 450°C annealed samples. For 1 and 2 hours annealed samples, the depth profile showed a contraction behavior. However, annealing for 4 hours at 450°C, V atoms started to diffuse again in silicon. This type of behavior has been observed previously in the diffusion behavior of Cr $1x10^{13}$ cm^{-2} implanted into silicon.

In fig. 5.7(a), SIMS profiles of Vanadium ions, 10^{13} cm^{-2} implanted and 550°C annealed samples for different time intervals, are presented. For 5 and 15 minutes annealing samples, V ions showed no diffusion. The profiles for 30 minutes and 60 minutes annealing samples showed a normal diffusion deep in silicon substrate. Fig. 5.7(b) presents SIMS profiles of V, $1x10^{12}$ cm^{-2} for as-implanted and 550°C annealed samples. For 5 minutes annealed sample the depth profile shows deep diffusion of the V ions in Si substrate, as the annealing time increases V ions show the same profile as for 5 minutes annealing sample. For 30 minutes and 60 minutes annealing samples, the peak is slightly higher than the peak for 15 minutes annealing sample but in general the figure showed normal diffusion due to the end of the range defects. Diffusivity of some V ions calculated using equation (5.1) and compared to previous work [SADO91], see table 5.1.

Table 5.1. The calculated diffusivities of V atoms in silicon

Dose (atoms/cm^2)	Annealing Time (hr)	Annealing Temperature (°C)	Diffusivity (cm^2/s) (our work)	Diffusivity (cm^2/s) (previous work)
1E12	1	550	1.09E-14	~ 9E-16 [SADO91]
1E13	1	550	4.91E-15	
1E13	4	450	3.83E-16	

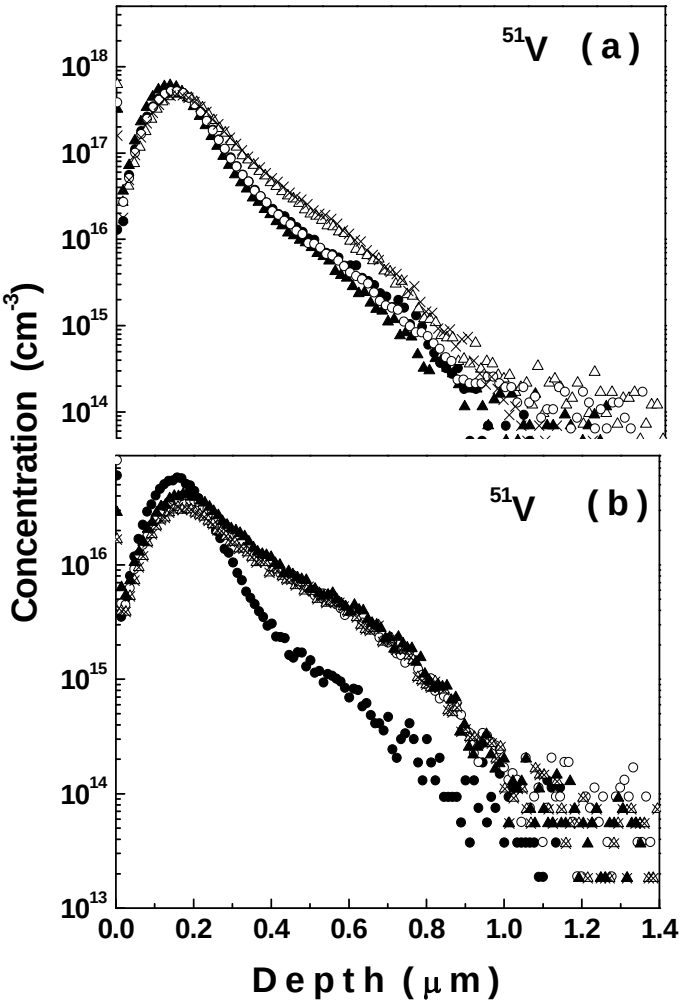

Figure 5.7 SIMS depth profiles (a) 10^{13} and (b) 10^{12} of ^{51}V cm^{-2} implanted with 200 keV into Si and annealed at 550°C for different times in Ar gas (● As-implanted, ○ 5 minutes, ▲ 15 minutes, Δ 30 minutes, × 60 minutes).

5.5. References

[BCHE04] A. Bchetnia, M. SouIssi, A. Rebey and B. El Jani, J. Crys. Grow. **270**, 376 (2004).

[CHAS97] E. Chason, S. T. Picraux,J. M. Poate, J. O. Boraland, M. I. Current, T. Diazde la Rubia, D. J. Eaglesham, O. W. Holland,M. E. Law, C. W. Magee, J. W. Mayer, J. Melngailis and A.F. Tasch, J. Appl. Phys. **81**, 6513 (1997).

[FAIR88] R.B. Fair, in Semiconductor Materials Processing Technology Handbook, edited by G.E. McGuire (Noyes, Park Ridge, N.J., 1988).

[FELD86] L. C. Feldman and J. W. Mayer, *Fundamentals of Surface and Thin Film Analysis*, North-Holand (1986).

[FISH99] D.J. Fisher*, Diffusion in Silicon*: 10 years of Research (Trans. Tech. Publications, 1999).

[FRAN01] H. Francois-Saint-Cyr, E. Anoshkina, F. Stevie, L. Chow, K. Richardson, and D. Zhou, J. Vac. Sci. Tech. B, **19**, 1769 (2001).

[GANT91]D. K. Gantom, Y. Nakano, K. Tada, Jpn. J. Appl. Phys. **30**, 1176 (1991).

[GRAF00] K. Graff, *Metal Impurities in Silicon-Device Fabrication* (2nd edition), Springer (2000).

[GRIE96] S. Griehl, M. Herms, J. Klober, J. R. Niklas, W.Siegel, Appl. Phys. Lett. **69**, 1767 (1996).

[HUGG72] H.L.Hugghes, R. D.Baxter, and B. Phillips, IEEE Trans. Nucl. Sci., NS-**19**, 256 (1972).

[ISTR00] A. A. Istratov, H. Hieslmair, and E. R. Weber, Appl. Phys. A, 70, 489 (2000).

[ISTR98]A. A. Istratov, C. Flink, H. Hieslmair, and E. R. Weber, Phys. Rev. Lett. **81**, 1243 (1998).

[ISTR99]A. A. Istratov, H. Hieslmair, and E. R. Weber, Appl. Phys. A, 69, (1999) 13.

[JOLY98] Jean-Pierre Joly, Microelectronic Engineering **40**, 285 (1998).

[JONE88] K. S. Jones, S. Prussin and E. R. Weber, Appl. Phys. A **45**, 1 (1988).

[JONE95]R. Jones, S. Oberg, J. Goss, P. R. Briddon, and A. Resende, Phys. Rev. Lett. **75**, 2734 (1995).

[JUN-T83] Juh-Tzeng Lue and O. Mayer, j. Appl. Phys. **54**, 1148 (1983).

[KIKO94] K. A. Kikoin and V. N. Fleurov, Transition Metal Impurities in Semiconductors, Electronic Structure and Physical Properties, World Scientific (1994).

[KONU91] B. Yu, N. Konuma, and E. Arai, J. Appl. Phys. **70**, 2408 (1991).

[KUTT84] W. Kutt, D. Dimderg, M. Maier, H. Karutle, F. Kohl, and E. Bauser, Appl. Phys. Lett. **44**, 1078 (1984).

[MAGE78] C. W. Magee and W. L. Harrington, Appl. Phys. Lett. **33**, 193 (1978).

[NAKA00] M. Nakamura, Appl. Phys. Lett. **76**, 2089 (2000).

[NAKA92] H. Nakashima and K. Hashimoto, Mater. Sci. Forum **83-87**, 227 (1992).

[OHSA90] J. Ohsaxa, H. Hakinki, H. Ikeda, M. Migi taka, J. Electrochem. Soc. **137**, 2608 (1990).

[SADO91] T. Sadoh and H. Nakashima, Appl. Phys. Lett. **58**, 1653 (1991).

[SCHR99] D. K. Schroder, *Semiconductor Material and Device Characterization*, John Willy& Sons (1999).

[SEIB88] M. Seibt and K. Graff, J. Appl. Phys. **63**, 4444 (1988).

[SHAC93]Y. Shacham-Diamand, A. Dedhia, D. Hoffstetter, and W. G. Oldham, J. Electrochem. Soc. **140**, 2427 (1993).

[SPIT89] F. H. M. Spit, D. Gupta, K. N. Tu, Phys. Rev. B, **39**, 1255 (1989).

[WEBE83] E. R. Weber, Appl. Phys. A **30**, 1 (1983).

[WILS80] R. G. Wilson, P. K. Vasudev, D. M. Jamba, C. A. Evans, Jr. and V. R. Deline, Appl. Phys. Lett. **36**, 215 (1980).

[WILS81] R. G. Wilson, Appl. Phys. **52**, 3954 (1981).

[XU88] F. Xu, D. M. Hill, Z. Lin, S. G. Anderson, Y. Shapira, J. H. Weaver, Appl. Phys. B **37**, 10295 (1988).

[YU91] S. Yu, T. Y. Tan and U.Gosele, J. Appl. Phys. **70**, 4827 (1991).

[ZHAN01] P. Zhang, Diffusion profiles of Chromium and Vanadium Ions Implanted into (100) Single crystalline Silicon, M.S. Thesis, University of Central Florida, (2001).

CHAPTER 6
DIFFUSION OF IMPLANTED SPECIES IN POLYCRYSTALLINE SILICON FILMS ON SILICON SUBSTRATE

6.1. Introduction

Poly-silicon is currently one of the materials at the heart of process development. This is due to its wide spread applications in solar cell devices, thin film transistors, and gate electrodes [RATH03]. Primarily in the solar cell industry, with a double digit annual growth rate in the last few years [WODI02], the feedstock of solar cells has shifted from the electronic grade silicon scrapes (or rejects) to poly-Si thin films or wafers. However, unlike crystalline silicon, poly-silicon (also known as multi-crystalline silicon) is seldom studied and there is need to obtain a diffusivity data in poly-silicon for device simulation and modeling. In this section, we report our experimental investigation of the diffusion behaviors of ten different elements implanted into poly-silicon thin films grown on silicon substrates.

There were a few reports [KNMI72] on the diffusion of impurities such as boron and phosphorus from oxide into poly-silicon. They found that both boron and phosphorus diffused more rapidly into poly-silicon than into single crystalline silicon. They related this enhanced diffusion to the grain boundary diffusion. In 1980, Hwang et al. [HWAN80] measured the grain boundary diffusion of Al in poly-silicon films by an Auger sputter profiling technique. They found that the grain boundary diffusion satisfied the Arrhenius-type equation, with $D^* = 1.3 \times 10^7$ cm^2/s and $Q_b = 2.64$ eV. Tseng et al. [TSEN92] on the other hand, studied the diffusion of F in poly-silicon films after implantation of F or BF_2. They found that F atoms were attracted more to the poly-silicon/SiO_2 interface as the annealing temperature increased and the narrowing of F distribution

in Si after thermal annealing. They related both phenomena to the low solubility of F in Si and the diffusion of F in poly-silicon is dominated by grain boundary diffusion. Very similar results regarding the distribution of F in Poly-silicon/Si systems were obtained by Chen et al. [CHEN95]. In 1995, Park & Schroder [PARK95] determined the diffusion coefficient of Cr in edge-defined film-fed-growth poly-silicon to be $2x10^{-17}$ cm^2/s at room temperature. They used Deep Level Transient Spectroscopy (DLTS) measurements to reveal that the grain boundaries are the main sources of deep-level impurities in the poly-silicon. Nakayama and Sakai [NAKA96] reported the redistribution of implanted N in poly-silicon and the segregation of N at the poly-silicon/SiO_2 interface and the SiO_2/Si interface. Others [MITC02] reported the Ge diffusion constant in poly-silicon and they found that it can be described by Arrhenius relationship with a pre-exponential factor of $D_o = 0.026$ cm^2/s and an activation energy of 2.59 ± 0.36 eV.

There have been several studies of the effect of contaminants on the photovoltaic properties of poly-silicon. Kalejs et al [KALE93] studied the effect of transition metal impurities on solar cell performance in poly-silicon thin film and they found that Ti and V have the most impact on the solar cell efficiency which can drop 35% at concentrations between 10^{13} and 10^{14} atoms/cm^3. For Mo and Cr, the degradation of solar cell efficiency is only 15% and 10%, respectively. In 2003, Istratov et al. [ISTR03] studied the impact of metal content on minority carrier diffusion length in poly-Si. They found that metal contaminations such as Fe, Ni, Co, Mo and Cr in poly-silicon do have concentrations sufficient to degrade the minority carrier diffusion length in poly-silicon to less than one micron.

6.2. Experimental Procedures

The poly-silicon film was grown on a p-type B doped silicon wafer, using a low-temperature chemical vapor deposition technique. The nominal thickness of the poly-silicon film is about 0.5μm. Impurity ions were implanted into this 0.5 μm Poly-silicon thin film at room temperature. The implantation energy and flux were tabulated in table 6.1. The ion implantation energy is chosen such that the peak of the impurity profile is in the middle of the poly-silicon film. Thermal anneals were carried out in a tube furnace at temperatures from 300°C to 1000°C, for 30 minutes each. Details of annealing procedures have been described in chapter 5, section 2.

Table 6.1. Implantation parameters.

Element	Energy (keV)	Dose (atoms/cm^2)
Be	70	1E14
Na	70	1E14
Cl	150	5E14
K	150	1E14
Ca	150	1E14
Ti	150	1E14
Cr	120	1.1E15
Mn	150	1.1E14
Ga	180	8E13
Ge	180	4.2E14

6.3. Results and Discussion

In fig.(6.1) we present the concentration depth profiles for Be, Na after annealing at different temperatures for 30 minutes. For Be as shown in fig. 6.1(a), the main features of the

concentration-depth are: (1) the trapping of Be atoms at the poly-Si/Si interface, and (2) the out-diffusion of Be atoms at 900°C and above. After 700°C anneal, the Be profile for the top 400 nanometers showed a flat distribution. Madar [MADA00] reported that Be is one of the few metals that doesn't form silicide, thus Be diffused out of silicon after annealing at higher temperature, 900°C and 1000°C. For Na ions, the diffusion behavior is very similar to that of Be ions, but Na traps at the poly-Si/Si interface seems to be more bonded. Wang et al [WANG97] studied recrystallization and diffusion for Na high dose implanted into single crystalline silicon using Rutherford backscattering spectrometry. They found Na segregation near the amorphous/ crystalline interface. After further annealing, they found the Na segregation dissolved by the grain boundary diffusion toward the surface. Our results, as shown in fig. 6.2(b), displayed very similar behaviors, including the trapping of Na near the poly-Si/Si interface and out-diffusion of Na through the grain boundary at high annealing temperatures. We can notice that there is still Na ions trapped at the poly-Si/Si interface and at the end-of range (EOR), between 200-300 nm.

In fig. (6.2), SIMS profiles for Ga and Cr implanted into poly-silicon are presented. If we look at the depth profiles, we can say that Ga and Cr seem not to have traps at poly-Si/Si interface and most of the Ga and Cr atoms left Poly-Si after anneal at 900°C or above. In 1990, Linnebach [LINN90] reported that the solubility of Ga ions in silicon changed from retrograde solubility at temperatures above 630°C to a non-retrograde solubility at temperatures below 630°C. This can explain our results, at low temperature the Ga ions tend to diffuse deeper into poly-silicon, while at high temperature Ga ions tend to diffuse out of the poly-silicon layer.

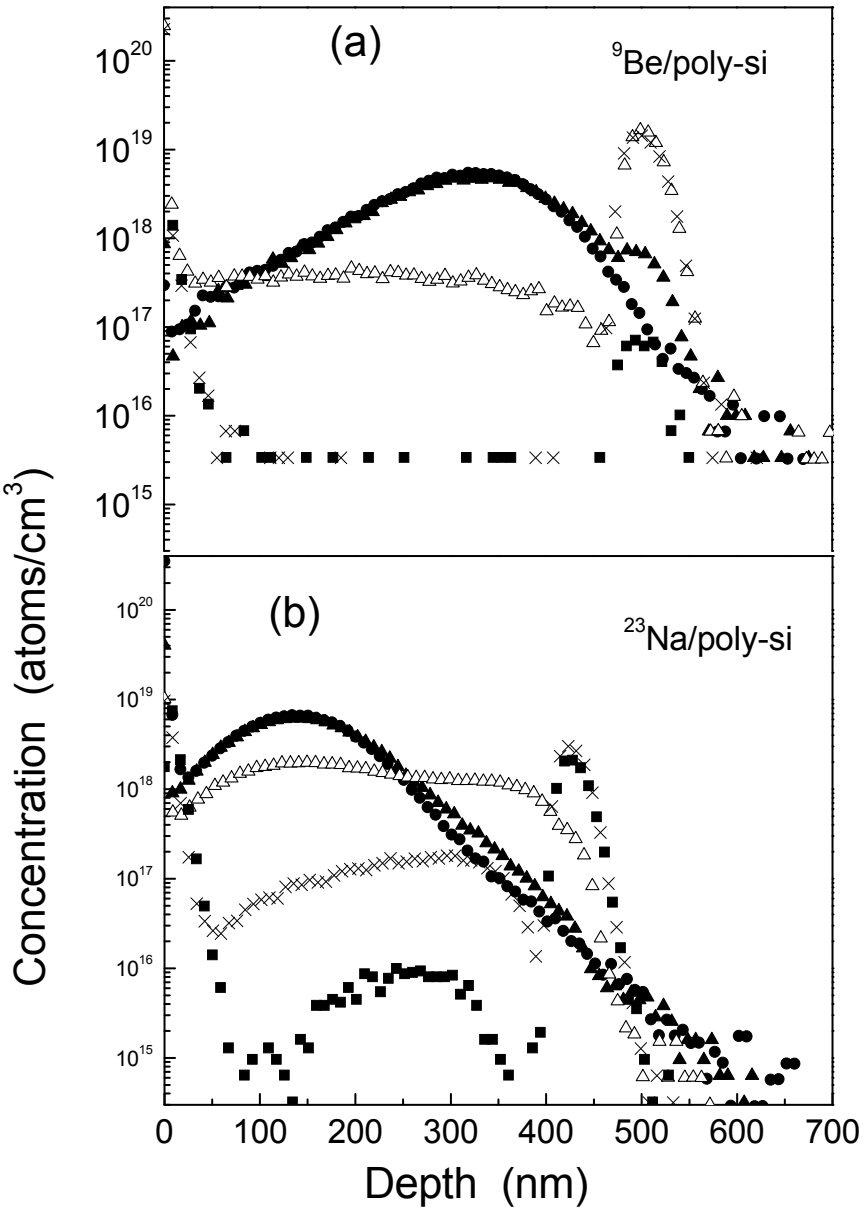

Figure 6.1. SIMS profiles of: (a) ^{9}Be (70 keV, 1E14 atoms/cm^2), (b) ^{23}Na (70 keV, 1E14 atoms/cm^2): (● As-implanted, ○ 300°C, ▲500°C, Δ 700°C, x 900°C, ■ 1000°C).

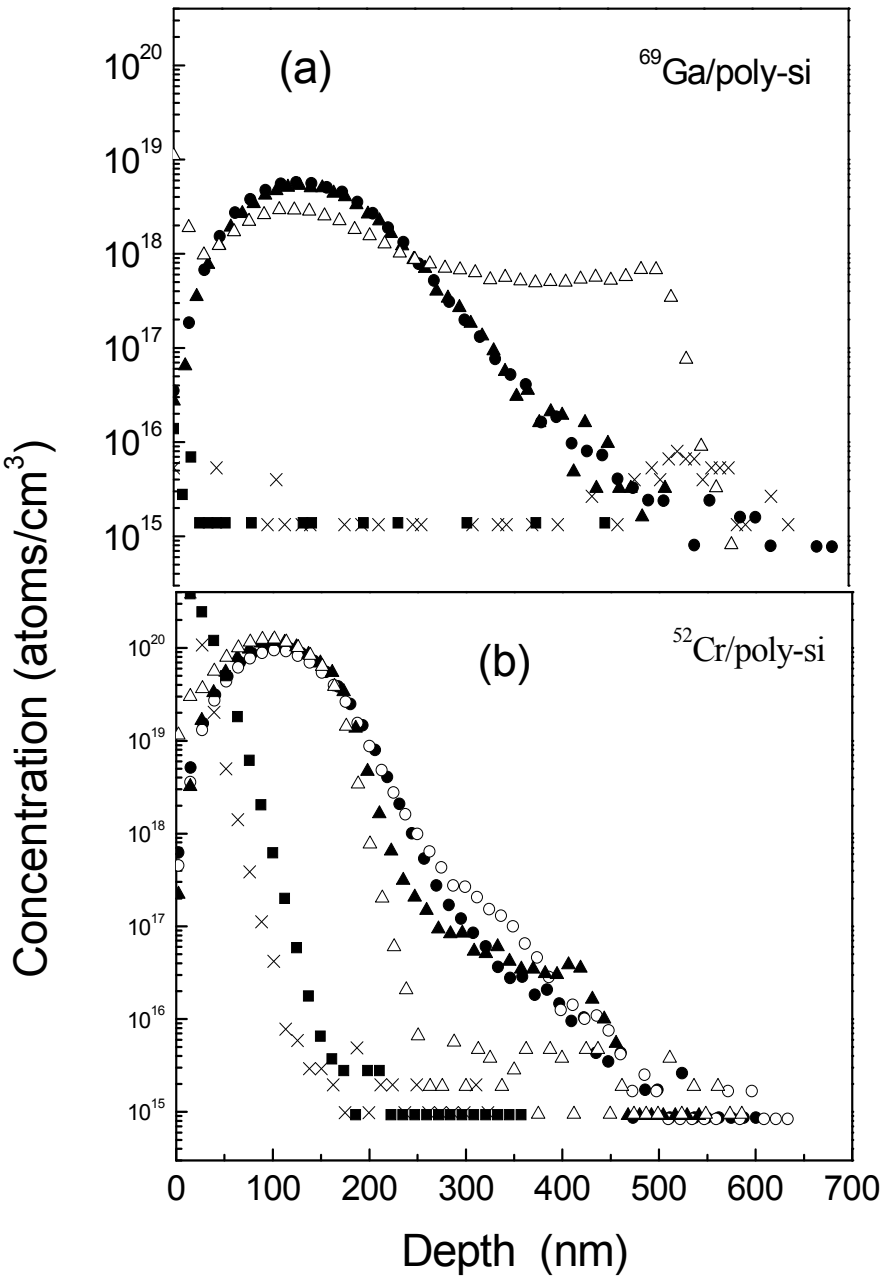

Figure 6.2. SIMS profiles of: (a) ^{69}Ga (180 keV, 8E13 atoms/cm^2), (b) ^{52}Cr (120 keV, 1E15 atoms/cm^2): (● As-implanted, ○ 300°C, ▲500°C, Δ 700°C, × 900°C, ■ 1000°C).

In Cr ions case, we can compare our present results with the recent work done by our group [ZANG04] on implanted Cr in single crystalline silicon. We can see that except that in poly-silicon host there is no solid phase epitaxial growth (SPEG), all other aspects of the migration of Cr into poly-silicon are similar to the single crystalline condition.

As we continue to study the diffusion behavior of more elements such as K, Ca, Ti and Ge into poly-silicon as shown in fig. (6.3) and fig. (6.4). We can see there is a main feature for depth profiles after annealing; these profiles showed that K, Ca, Ti and Ge atoms diffuse deeper into poly-silicon as the annealing temperature increased. Except Ge, these ions seem to be trapped by poly-Si/Si interface at 500 nm. From the phase diagram of Ge-Si [CHEN95], Ge is fully miscible with silicon, which may explain why there are no traps for Ge at poly-Si/Si interface. In this section we will report the diffusivity of these 4 elements using a simple procedure that has been previously documented [OMME85, OMME87]. We assume that the impurity concentration will have a joint half Gaussian distribution and we will use the concentration profile from the peak to the poly-Si/Si interface for the calculation of diffusion coefficients. The concentration profile after anneal is given by equation (6.1).

$$C(x) = C_O \exp\left(\frac{-(x - x_m)^2}{2(\sigma^2 + 2Dt)}\right) \tag{6.1}$$

Where x_m is the peak position and σ is the standard deviation of the concentration depth profile, D and t are the diffusion coefficient and the diffusion time. The results for the diffusion coefficients are given in table 6.2. Form the table we can see that the diffusion coefficient of Ge at 700°C in poly-silicon is much larger than that in the crystalline silicon, for K and Ti, the

diffusion coefficients in poly-silicon are either comparable or much smaller than that in the crystalline silicon.

Table 6.2. Diffusion coefficients at 700°C of several elements in silicon and poly-silicon.

Element	D (cm^2/s) in silicon (from literature)	D_{APP} (cm^2/s) in poly-silicon (present work)
K	$1.3x10^{-7}$ [BEAD85]	$6.6x10^{-15}$
Ca	~	$2.1x10^{-14}$
Ti	$3.4x10^{-13}$ [BOLD77]	$1.25x10^{-14}$
Ge	$2.7x10^{-22}$ [BEAD85]	$3.3x10^{-16}$

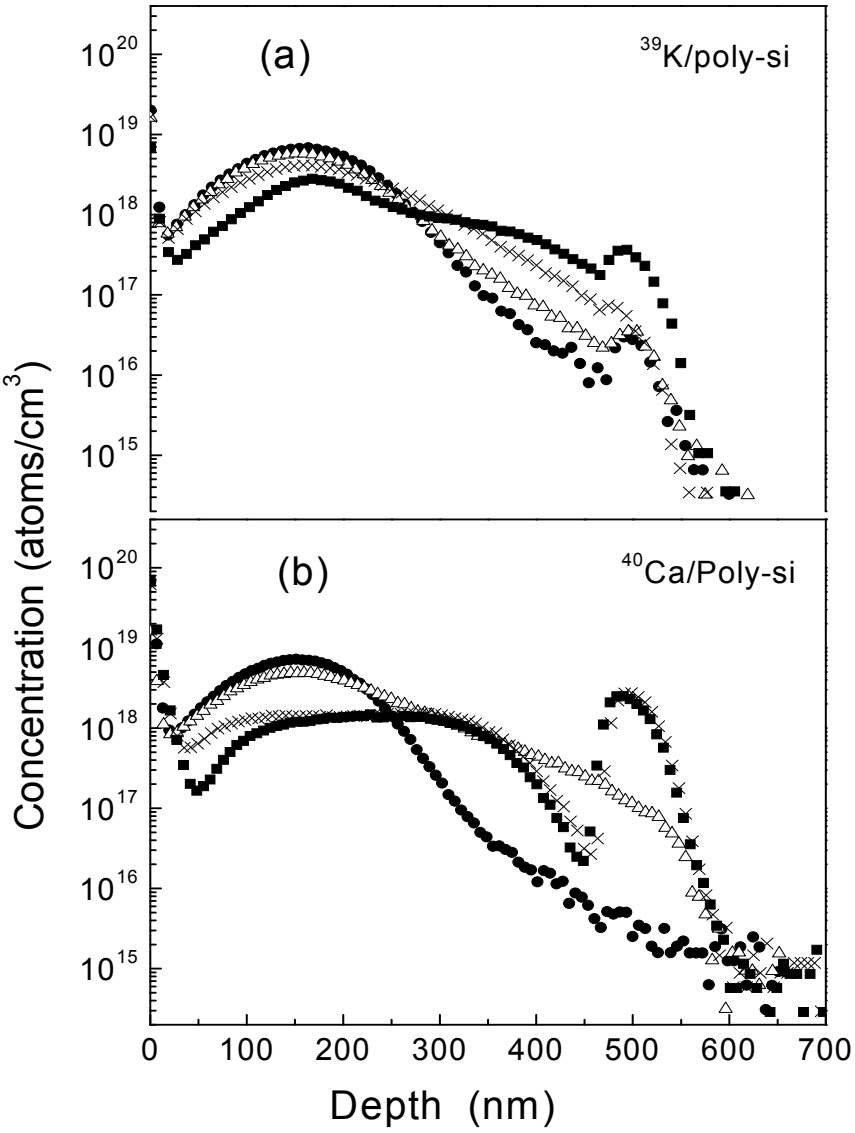

Figure 6.3 SIMS profiles of: (a) ^{39}K (150 keV, 1E14 atoms/cm^2), (b) ^{40}Ca (150 keV, 1E14 atoms/cm^2) : (● As-implanted, Δ 700°C, × 900°C, ■ 1000°C).

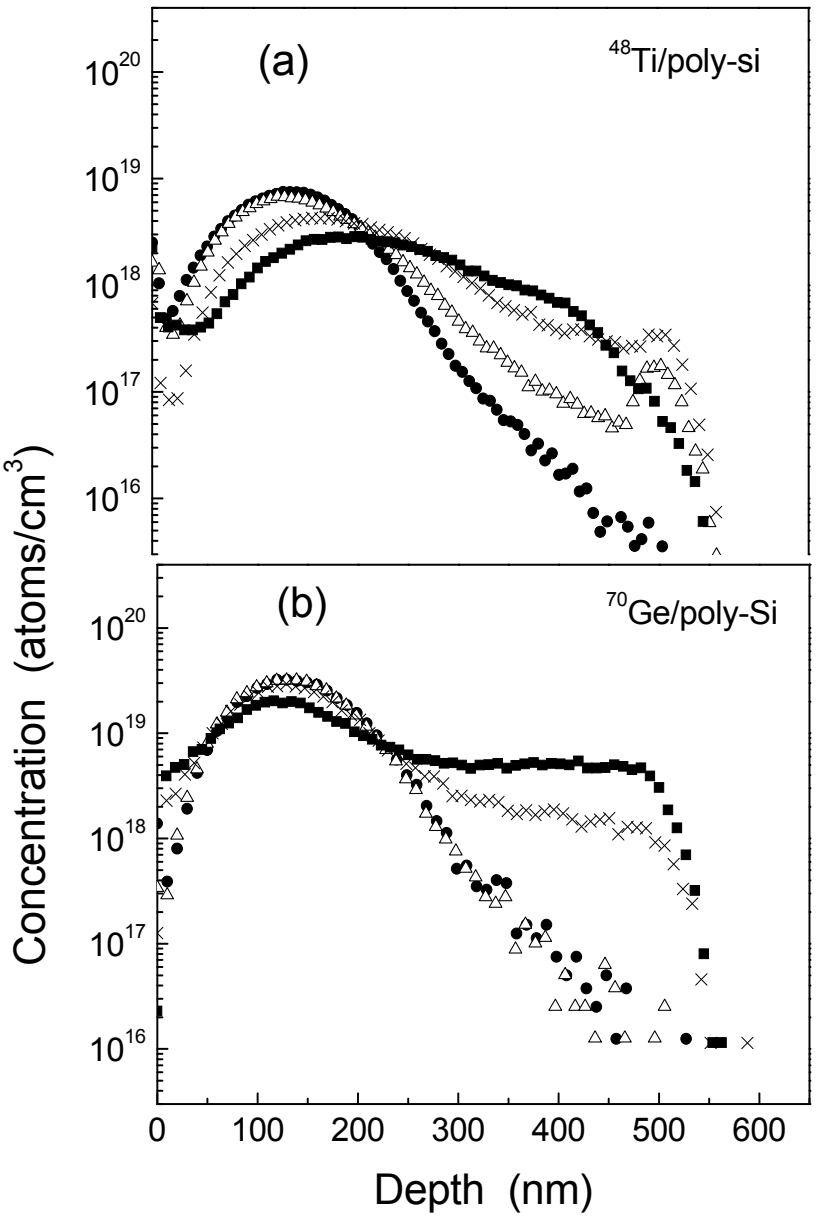

Figure 6.4. SIMS profiles of: (a) 48Ti (150 keV, 1E14 atoms/cm2), (b) 70Ge (180 keV, 4.2E14 atoms/cm2): (● As-implanted, Δ 700°C, × 900°C, ■ 1000°C).

Fig. (6.5) presents the concentration-depth profiles of Cl and Mn for as-implanted and thermal anneal. The main characteristic in these two profiles is the contraction of the concentration

profiles after anneal. In the case of Cl as shown in fig. 6.5(a), the atoms get trapped at the poly-Si/Si interface. The as-implanted sample showed a factor of 50 raise in the Cl concentration at the poly-Si/Si interface as compared with the background. This is due to the use of Cl in the sample preparation. After annealing at 700°C, the concentration of Cl atoms became greatly wider at 180 nm. For 900°C and 1000°C annealed samples, the concentration near the surface (20 nm-150 nm) was all gone, causing the concentration gradient even larger than the as-implanted sample. Tseng et al [TSEN92] have shown that the contraction of Fluorine profile under anneal can be explained by grain boundary diffusion based on networks. Cl diffusion profiles were very similar to that observed for F diffusion behaviors.

Fig. 6.5(b), shows SIMS profiles of Mn for as-implanted and annealed samples. After 700°C anneal, the Mn concentration Peak slightly shifted toward the surface and the distribution become much narrower. After 900°C anneal, the Mn concentration peak shifted significantly toward the poly-Si/Si interface and the distribution also became narrower. This is caused by the depletion of Mn atoms near the surface region. For 1000°C annealed sample, almost all Mn atoms diffused out of poly-silicon layer. This is a very complex behavior which can't be understood through a simple diffusion model. We have to take into account the interaction between the damages and the defects created by ion implantation and the formation of silicide need to be considered.

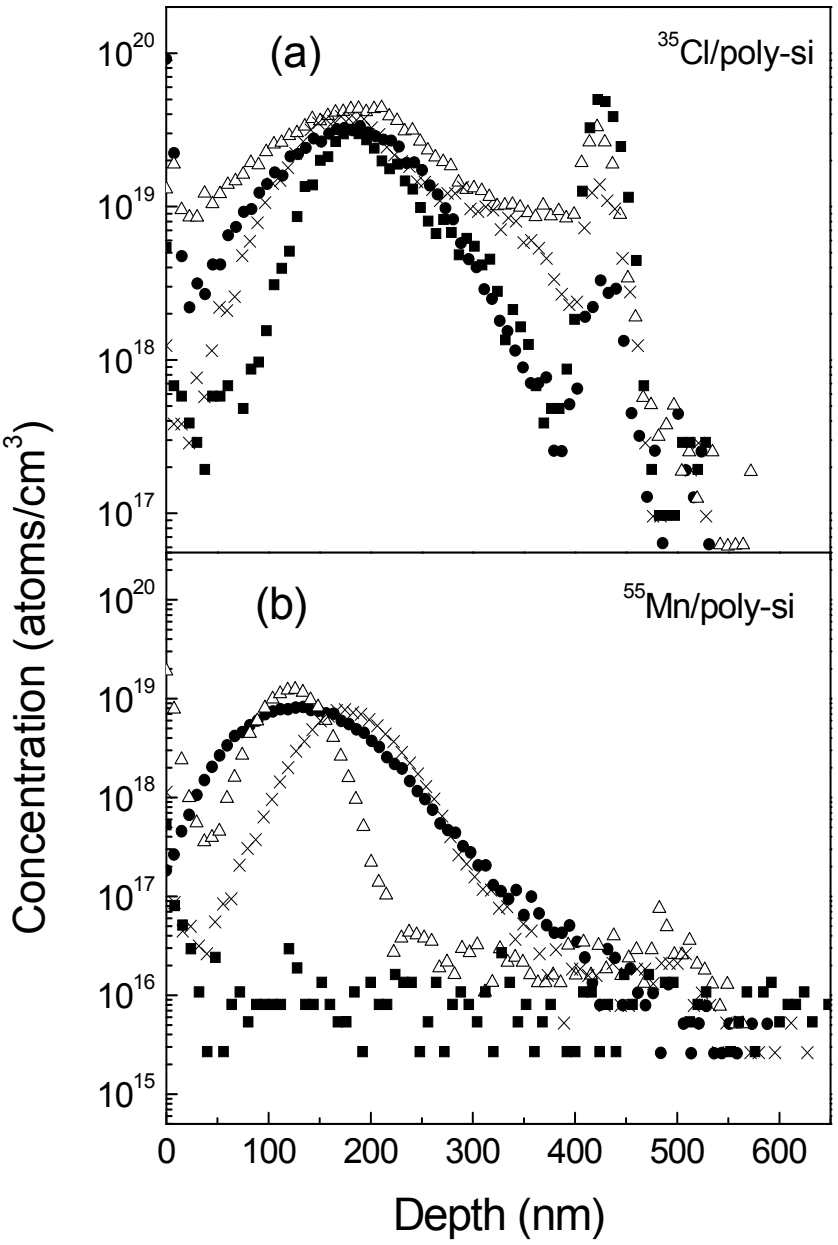

Figure 6.5. SIMS profiles of: (a) ^{35}Cl (150 keV, 5E14 atoms/cm^2), (b) ^{55}Mn (150 keV, 1.1E14 atoms/cm^2): (● As-implanted, Δ 700°C, × 900°C, ■ 1000°C).

6.4. Summary

Ten different elements were implanted into poly-silicon films deposited on a silicon substrate using ion implantation. The diffusion behavior of as-implanted and annealed samples was characterized using SIMS. The concentration-depth profiles show very complex behaviors. The apparent calculated diffusivities for some elements such as K and Ti in poly-silicon are either comparable or much smaller than that in the crystalline silicon. In contrast, the diffusion coefficient of Ge at 700°C in poly-silicon is much larger than that in the crystalline silicon,

In poly-silicon, there are two main types of diffusion: (1) bulk diffusion, and (2) grain boundaries diffusion. According to our study, the grain boundary can enhance the diffusion or provide guttering sites to trap the impurities at the grain boundaries.

6.5. References

[BEAD85] W. E. Beadle, J. C. C. Tsai, and R. D. Plummer, *Quick Reference Manual for Silicon Integrated Circuit Technology* (Wiley, New York, 1985).

[BOLD77] V. P. Boldyrew, F. I. Prokovskii, S. G. Romanovskaro, A. V. Tkach, and I. E. Shimanovich, Sov. Phys. Semicond. **11**, 709 (1977).

[CHEN95] T.P. Chen, T.F. Lei, C.Y. Chang, W.Y. Hsieh, and L.J. Chen, J. Electrochem. Soc. **142**, 2000 (1995).

[HWAN80] J.C.M. Hwang, P.S. Ho, J.E. Lewis, and D.R. Campbell; J. Appl. Phys. **51**, 1576 (1980).

[ISTR03] A. A. Istratov, T. Buonassisi, R.J. McDonald, A.R. Smith, R. Schindler, J. P. Kalejs and E. R. Weber, J. Appl. Phys. **94**, 6552 (2003).

[KALE93] J.P. Kalejs, B.R. Bathey, J.T. Borenstien, and R.W. Stormont, Twenty-third IEEE PVSC, 184 (1993).

[KNMI72] T.I. Kamins, J. Manoliu, and R.N. Tucker; J. Appl. Phys. **43**, 83 (1972).

[LINN90] R. N. Linnebach, J. Appl. Phys. **67**, 6794 (1990).

[MADA00] R. Madar, in "*Silicides: Fundamentals and Applications*"*, edit by* L. Migillo and F. d'Heurle, Singapore, New Jersy, London, Hong Kong, World Scientific (2000).

[MITC02] M.J. Mitchell, P. Ashburn, and P.L.F. Hemment, J. Appl. Phys. **92**, 6924 (2002).

[NAKA96] S. Nakayama and T. Sakai, J. Appl. Phys. **79**, 4024 (1996).

[OMME85] A. H. van Ommen, J. Appl. Phys. **57**, 1872 (1985).

[OMME87] A. H. van Ommen, J. Appl. Phys. **61**, 933 (1987).

[PARK95] S.H. Park, and D.K. Schroder; J. Appl. Phys. **78**, 801 (1995).

[RATH03] J. K. Rath, Solar Energy Materials & Solar Cells **76**, 431 (2003).

[TSEN92] H.H. Tseng, M. Orlowski, P.J. Tobin, and R.L. Hance, Electron Device Letters **13**, 14 (1992).

[WANG97] W. H. Wang, W. Bolse, C. Illgner, K. P. Lieb, J. Keinonen, and J. C. Ewert, Thin Solid Films **295**, 169 (1997).

[WODI02] P. Woditsch and W. Koch, Solar Energy Materials & Solar Cells **72**, 11 (2002).

[ZANG04] P. Zhang, F. Stevie, R. Vanfleet, R. Neelakantan, M. Klimov, D. Zhou, and L. Chow, J. Appl. Phys. **96**, 1053 (2004).

CHAPTER 7
THE ANNEALING BEHAVIOR OF IMPLANTED ELEMENTS INTO TANTALUM SILICIDE

7.1. Introduction

Silicides are compounds of silicon with more electropositive elements in the periodic table. Silicides are called intermetallic materials, which means, it behaves more or less like metals. In 1960, transition-metal silicides attracted attention of many researchers because of their useful applications in Silicon Integrated Circuits (SICs) industry. Silicides are used as conductors in SICs because of their useful properties such as: Their corrosion resistance, their stability under higher temperature and lower electrical resistivity[MURA80].

Researchers used different techniques to produce silicide materials; they used powder metallurgical techniques in 1950s through 1960s [KEIF63, WEHR67]. Currently, there are two main methods which have been used to form silicides in semiconductor technology. The first is called metal/Si couples; the metal is deposited on Si wafer, then annealed to let the silicon react with the metal. The second is "Co-deposited material" method, where metal and silicon are sputtered to form a silicide layer on top of the substrate [READ92, MURA90]. Silicide layer is formed by either sputtering of separate metal and silicon targets or by a composite metal-silicon target. In our study, the co-sputtering is the method used to form silicide layer on top of silicon.

There are several works done on diffusion in silicide. Wittmer et al. [WITT84] studied the low temperature diffusion of dopant atoms in silicon during interfacial formation. They found that diffusion enhancement occurs only during interfacial formation of near-noble-silicides such as

PtSi, Pd_2Si and NiSi but not refractory-metal silicides such as TiSi, $TiSi_2$, VSi_2 and $TaSi_2$. Maex et al. [MAEX89] investigated the stability of the doped Si with respect to contacting silicides. They reported that high concentration As and B-doped Si were unstable underneath overlaying silicide layers. Myers et al. [MYER96] studied the implantation-formed cavities and boron-silicide precipitates as strong segregation gutter for transition metals. They found that both of cavities and precipitates appear to be promising. Others [ZARI96] tried to analyze thermal modifications of impurity profile implanted into silicide films to get estimation for the volume diffusion. The interpretation and the values of volume diffusion coefficients was confirmed by analyzing B profile implanted into bulk samples [ZARI96]. They found that the values of the volume diffusion coefficient for most dopants and silicides are similar to Si (Ge) self diffusion coefficient which means the diffusion mechanism should be similar (vacancy mechanism). However, B diffusion into $CoSi_2$ is three orders of magnitude faster than Si (Ge) self diffusion. Due to the size of B atoms and the open structure of $CoSi_2$, a strong contribution of interstitial diffusion is expected. Most diffusion results into silicon reached an important point, whatever the dopant and the silicide considered, dopant diffusion into silicides is several orders of magnitude faster than in Si. The transport of the dopants in a silicides/Si structure is restricted by diffusion in Si. This means that the distribution in a silicide/Si structure is limited by diffusion into silicon. In this chapter, we focus on the diffusion behaviors of 11 elements into 500 nm $TaSi_2$ deposited on Si substrate. These are: K, Ca, Ti, V, Cr, Mn, Na, Cl, Be, Ga, and Ge. Secondary ion mass spectrometry is used to obtain the concentration-depth profiles after thermal annealing.

7.2. Experimental Procedures

A poly-crystalline Tantalum silicide ($TaSi_2$) thin film is prepared on top of (100) silicon substrate using co-sputtering. The Si/Ta ratio was typically 2.2 to 2.6 as measured by Rutherford backscattering Spectrometry (RBS) [STEV89]. The thickness of the silicide layer is about 500 nm thick. Ion implantation is used to implant K, Ca, Ti, V, Cr, Mn, Na, Cl, Be, Ga and Ge ions into the silicide layer. The implantation energy and the dosages are listed in table 7.1. Thermal annealing is carried out as mentioned earlier in chapter 5, section 2. SIMS was used to analyze the concentration-depth profiles.

Table 7.1. Implantation Parameters.

Element	Energy (kev)	Dose (atoms/cm^2)
Be	70	1E14
Na	70	1E14
Cl	150	5E14
K	150	1E14
Ca	150	1E14
Ti	150	1E14
V	150	1E14
Cr	120	1.1E15
Mn	150	1E14
Ga	180	8E13
Ge	180	4.2E14

7.3. Results and Discussion

In fig. (7.1), we present the concentration-depth profiles of K and Ca implanted into 500 nm $TaSi_2$. Fig. 7.1(a) shows SIMS profiles of K ions for as-implanted and annealed at 700, 900 and 1000°C for 30 minutes. Depth profiles show no diffusion at 700 and 900°C, while K ions started to diffuse more into the silicide layer at 1000°C. The data indicate that K doesn't diffuse fast in silicide while in poly-silicon, K ions diffuse faster as shown in chapter 6. Fig. 7.1(b) presents rather different depth profiles of Ca ions implanted into $TaSi_2$. The as-implanted and 700°C annealed samples show the same depth profile, which means that there is no diffusion for Ca ions up to 700°C. SIMS profiles for 900 and 1000°C annealed samples show movement of Ca atoms into the silicide layer. At 900°C, we noticed that Ca diffused to about 275 nm and then decreased rapidly, while at 1000°C the ions mostly diffused through the entire silicide layer.

Fig. (7.2) shows the depth profiles for Ti and V implanted into $TaSi_2$ for as-implanted and annealed samples for 30 minutes. Fig. 7.2(a) presents SIMS depth profiles of Ti ions implanted into $TaSi_2$. The as-implanted, 300 and 500°C depth profiles show almost no movement of the implants. At 700°C, we observed diffusion in the silicide layer. Annealing at higher temperatures, 900°C and 1000°C, Ti ions display flat concentration profile in the silicide layer. At 500 nm depth, the concentration profile shows a step due to the differences in the solubility and the diffusivity behavior of Ti in silicide and in silicon. From fig. 7.2(b), we find that the V ions have a diffusion behavior similar to Ti. For as-implanted, 300 and 500°C, V doesn't show any movement inside the silicide layer except at 700°C, we detect diffusion behavior at 200 nm depth. At 900, and 1000°C, the depth profiles show complete diffusion of V into silicide. All the implanted ions distributed equally inside the silicide layer.

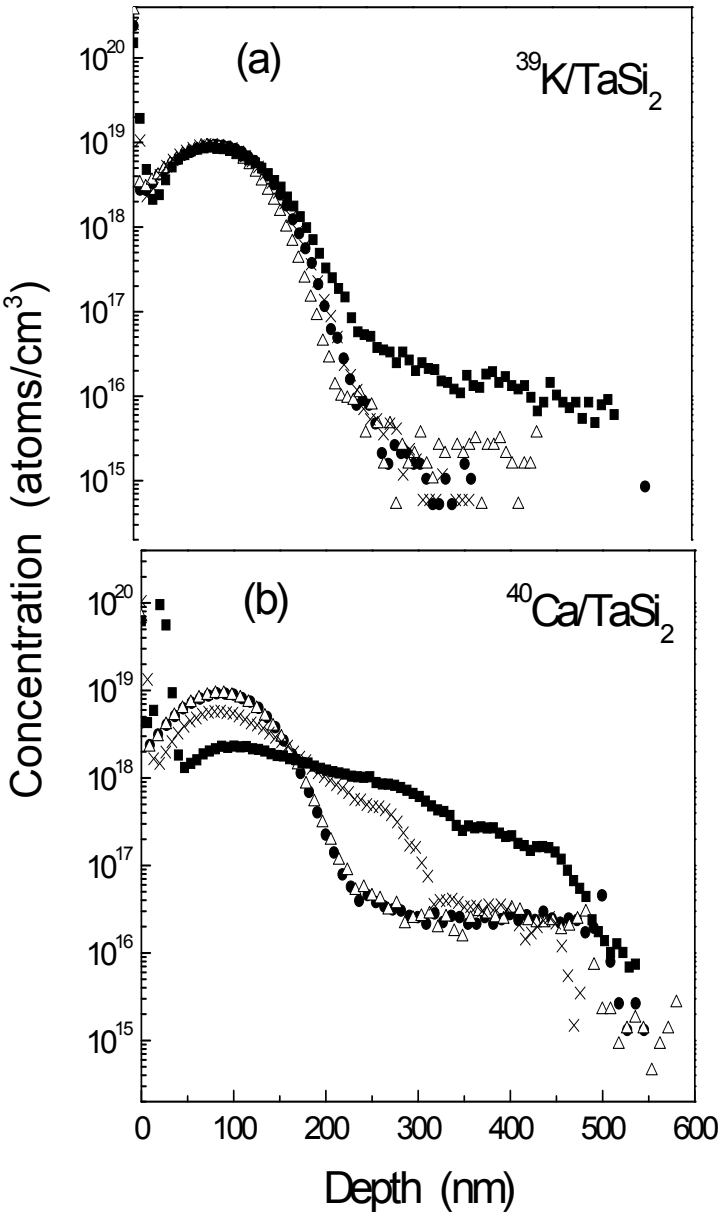

Figure 7.1 SIMS profiles of: (a) ^{39}K (150 keV, 1E14 atoms/cm^2), (b) ^{40}Ca (150 keV, 1E14 atoms/cm^2): (● As-implanted, Δ 700°C, × 900°C, ■1000°C).

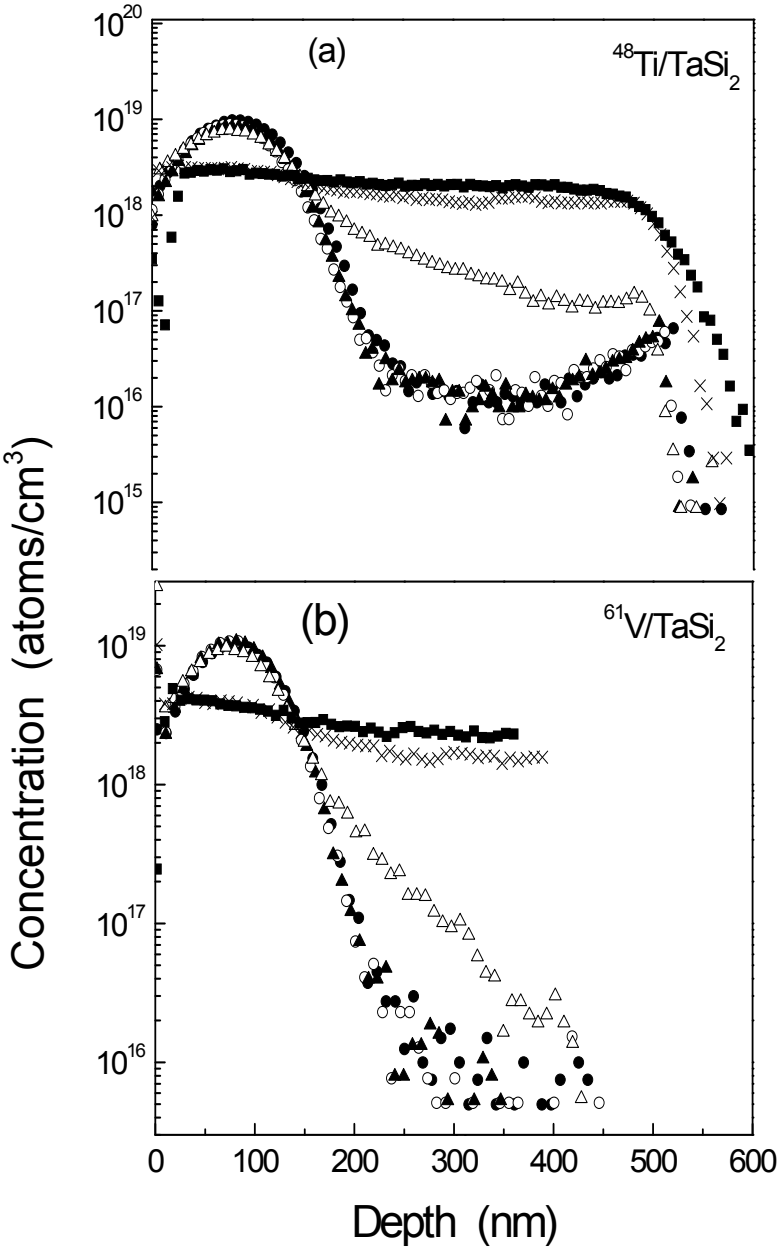

Figure 7.2 SIMS profiles of: (a) ^{48}Ti (150 keV, 1E14 atoms/cm^2), (b) ^{61}V (150 keV, 1E14 atoms/cm^2): (● As-implanted, ○ 300°C, ▲500°C, Δ 700°C, × 900°C, ■ 1000°C).

Fig. (7.3) shows concentration profiles of Cr and Mn implanted into $TaSi_2$. As shown in fig. 7.3(a) and 7.3(b), Cr and Mn depth profiles show no movements of the implanted ions at 300 and 500°C-annealed samples. At 700°C-annealed sample, Cr ions started to show movements at 150 nm depth. Annealing at higher temperatures such as 900°C and 1000°C, Cr and Mn ions show flat diffusion profile inside the silicide layer.

As we continued to study the diffusion behavior of more elements; fig. (7.4) presents SIMS depth profiles of Be, Ga and Ge ions implanted into $TaSi_2$. The general observation is that all of these elements distribute evenly starting at 500°C inside the silicide layer. Fig. 7.4(a) shows the concentration-depth profile of Be ions for as implanted and annealed samples for 30 minutes. As shown, no movements for Be ions inside the silicide layer for 300°C-annealed sample but started to diffuse at 500°C and 700°C. Be ions distributed evenly inside the silicide layer. There is a bump showing around 345 nm for 500°C due to preparation condition of the silicide layer as explained in [STEV89], where the first target used out and replaced. At 700°C, some Be ions moved to the surface and the concentration increased from around $1x10^{18}$ to around $5x10^{20}$ atoms/cm^3. The rest of the ions are distributed evenly and deeper inside the silicide layer. The step at 500 nm at the interface is due to the difference in the solubility limit of silicide and silicon.

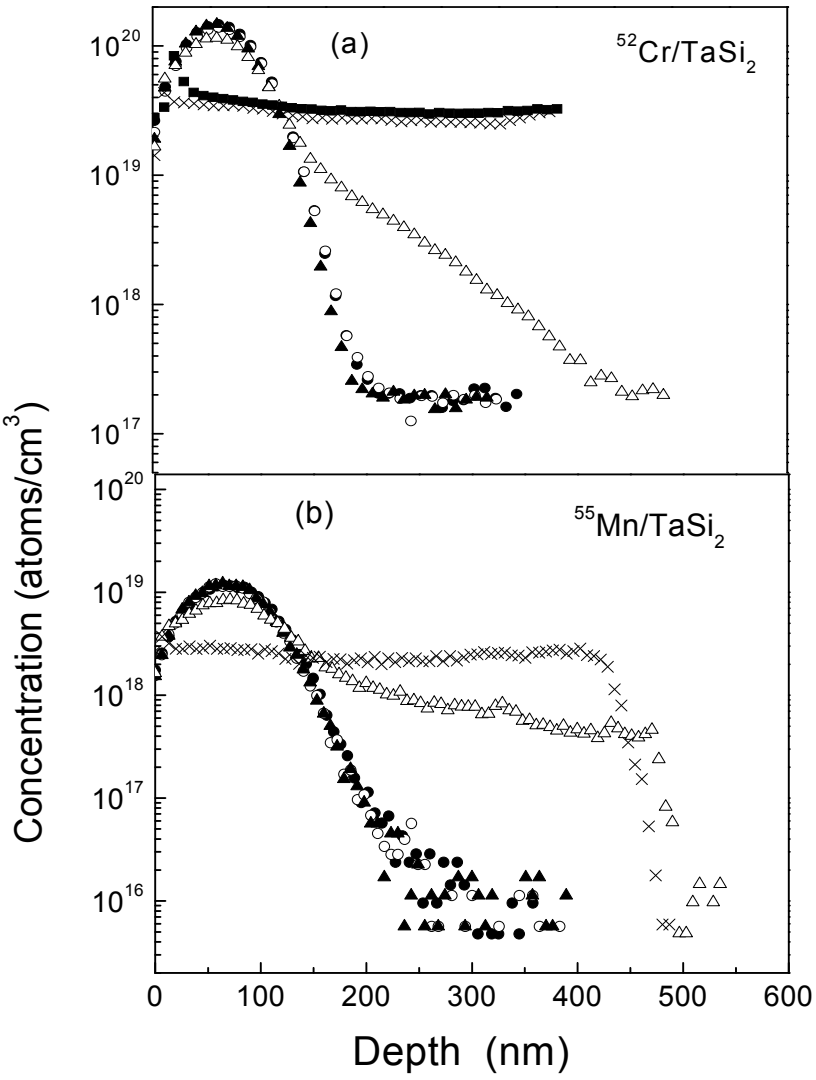

Figure 7.3 SIMS profiles of: (a) ^{52}Cr (120 keV, 1.1E15 atoms/cm^2), (b) ^{55}Mn (180 keV, 4.2E14 atoms/cm^2): (● As-implanted, ○ 300°C, ▲500°C, Δ 700°C, × 900°C, ■ 1000°C).

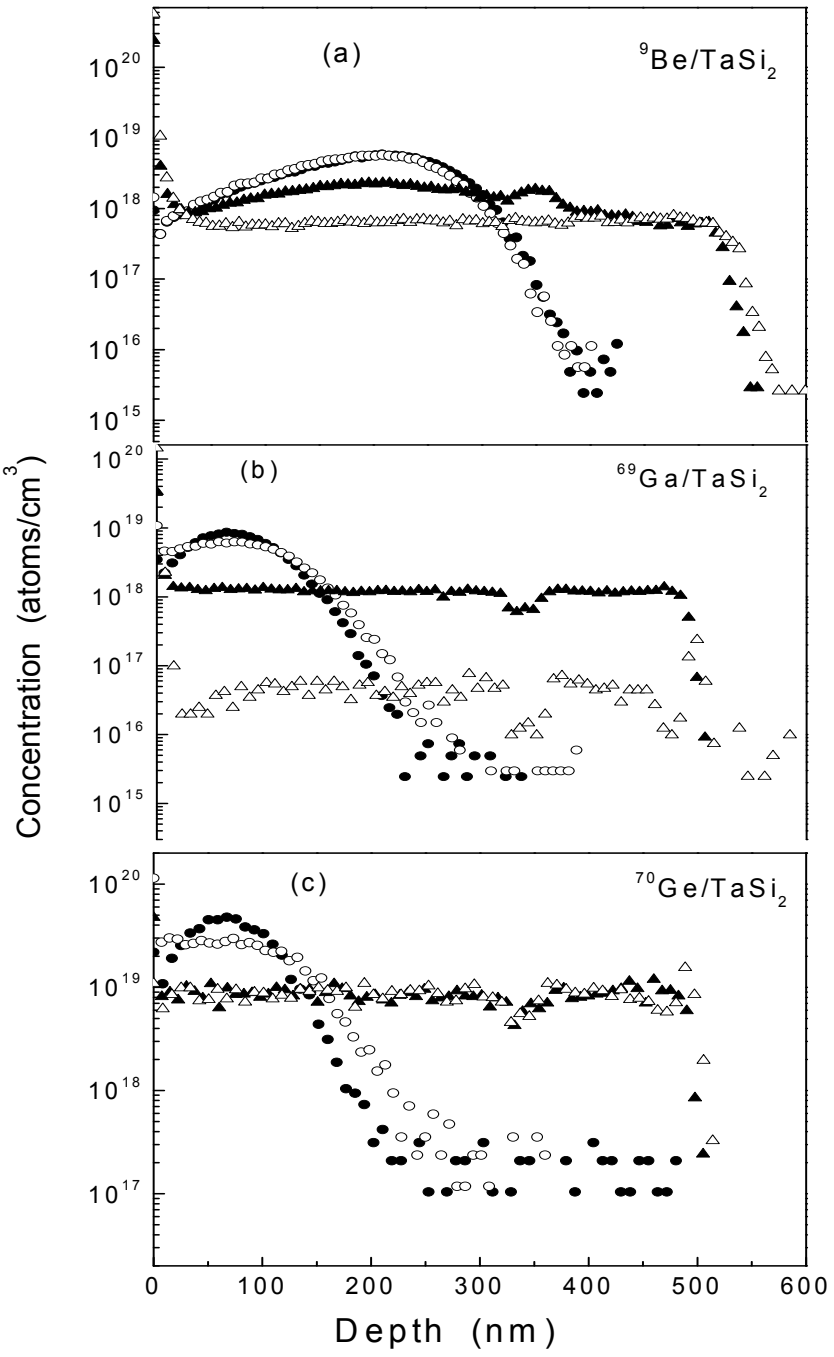

Figure 7.4 SIMS profiles of: (a) ^{9}Be (70 keV, 1E14 atoms/cm^2), (b) ^{69}Ga (180 keV, 8E13 atoms/cm^2), (c) ^{70}Ge (180 keV, 4.2E14 atoms/cm^2): (● As-implanted, ○ 300°C, ▲500°C, Δ 700°C).

Fig. 7.4(b) show the distribution profile of Ga dopants inside the silicide layer using SIMS. We found that Ga ions have the same general behavior as Be and Ge ions. At 300°C, dopants started to show almost normal diffusion profile. For 500°C and 700°C-annealed samples, SIMS profile show an even distribution for Ga atoms and a dramatic decrease in the concentration inside the silicide layer at 500°C. The dip showing around 350nm is due to the preparation condition [STEV89]. For Ge ions, fig. 7.4(c) shows the concentration-depth profiles of as-implanted and the annealed samples at 300-700°C for 30 minutes. At 300°C, SIMS profile shows normal diffusion inside the silicide layer. Annealing at 500°C and 700°C, the concentration-depth profile shows an even distribution for the Ge atoms inside the silicide layer and there is almost no change in the depth profile.

Fig. (7.5) presents SIMS depth profiles for Na and Cl ions implanted into $TaSi_2$ for as-implanted and annealed at 700-1000°C for 30 minutes. Fig. 7.5(a) presents a concentration-depth profile for Na ions which is representing a similar distribution behavior of Ca ions inside $TaSi_2$. The as-implanted and 700°C-annealed samples show almost the same depth profile, which means that there is no movement for Na ions up to 700°C, while annealing at 900°C and 1000°C show movement of Na atoms into the silicide layer. At 900°C, we notice that Na diffused to about 275 nm and then decreases rapidly, while at 1000°C, the ions diffused through the entire silicide layer. The concentration of Na ions increased at the surface at higher temperatures. The alkali and alkali earth metals such as Na and Ca appear to have almost the same distribution behavior inside the silicide layer.

Cl is an element of the halogen family, scarcely dissolve in liquids. It seems to have the same behavior inside the silicide layer. There is almost no movement up to 900°C as shown in fig. 7.5(b). At higher temperatures such as 1000°C, the depth profile shows more diffusion of Cl atoms into the silicide layer. We noticed that Cl ions behavior within 50 nm deep in the silicide layer was complex. The ions closer to the surface tend to diffuse out, while the ions closer to the end of the range tend to diffuse deeper.

7.4. General Conclusion

we studied the diffusion behavior of alkali metals, alkali earth metals, transition metals, other metals and halogen. Some of these elements show fast diffusion into silicide layer. Other elements show diffusion at higher temperatures, rather than lower temperatures. In general we conclude that the impurities diffusion in silicides is more than in poly-silicon and silicon due to different factors including grain boundaries, silicide/silicon interface, and bulk diffusion.

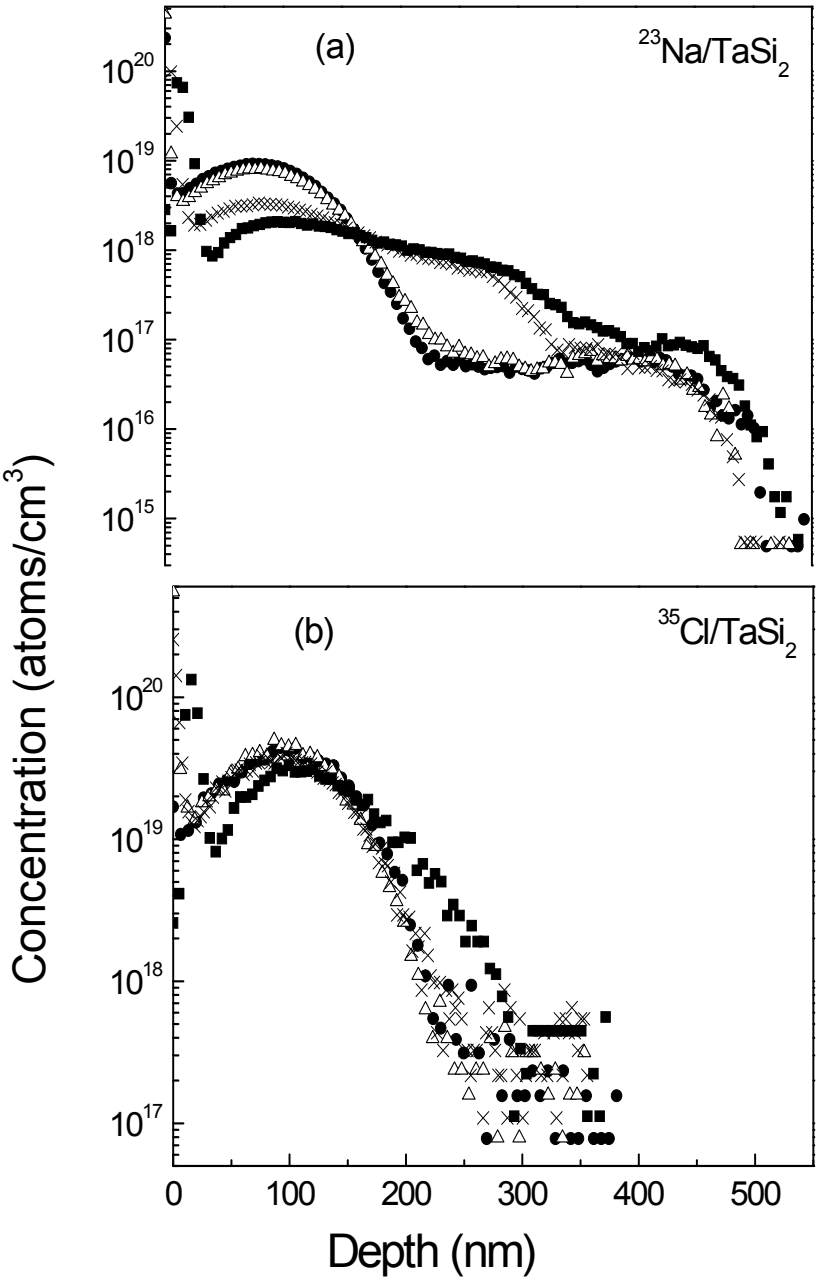

Figure 7.5 SIMS profiles of: (a) ^{23}Na (70 keV, 1E14 atoms/cm^2), (b) ^{35}Cl (180 keV, 5E14 atoms/cm^2): (● As-implanted, Δ 700°C, × 900°C, ■ 1000°C).

7.5. References

[KEIF63] R. Keiffer and F. Benesovsk, Hartstoffe, Spring-Verlag, Wien, 455 (1963).

[MAEX89] K. Maex, R. F. De Keersmaecker, G. Ghosh, L. Delaey and V. Probst, J. Appl. Phys. **66**, 5327 (1989).

[MURA80] S. P. Murarka, J. Vac. Sci. Technol. **17**, 775 (1980).

[MURA90] S. P. Muraka. Phys. Rev. Lett. **64**, 117 (1990).

[MYER96] S. M. Myers, G. A. Petersen, D. M. Follstaedt, T. J. Headley, J. R. Michael and C. H. Seager, Nuclear Instruments and Methods in Physics Research Section B, **120**, 43 (1996).

[READ92] A. H. Reader and A. H. ven Ommen, P. J. W. Wejis, R. A. M. Wolters and D. J. Oostra, Rep. Prog. Phys. **56**, 1397 (1992).

[STEV89] F. A. Stevie and P. M. Kahora, and G. W. Cochran, J. Vac. Sci. Technol. A **7**, 1539 (1989).

[WEHR67] R. Wehrmann, *High-temperature Materials and Technology, edit by* I. E. Campbell and E. M. Sherwood, Wiley,New York, 399 (1967).

[WITT84] M. Wittmer and K. N. Tu. Physical Review B, 29, (1984), 2010.

[ZARI96] C. Zaring, A. Pisch, J. Cardenas, P. Gas and B. G. Svensson, J. Appl. Phys. **80**, 2742 (1996).

CHAPTER 8
ANNEALING BEHAVIOR OF IMPLANTED LI IONS IN GAN THIN FILMS ANALYZED BY SECONDARY ION MASS SPECTROMETRY

Doping of semiconductors by ion implantation presents many advantages in comparison with doping during film growth. These include: (i) Almost all elements can be implanted with adequately high purity, and (ii) The concentration and depth distributions of the dopants are exactly controllable. However, this process is accompanied by defects and damages which has to be removed by the use of annealing treatments. In the case of gallium nitride (GaN), the annealing procedure for dopant activation is very complicated due to the decomposition of the GaN surface for temperatures above 900°C [KING98, VART96 and AMBA98]. Annealing temperatures of around 1300°C for >5 minutes are necessary for GaN to fulfill the rule of thumb stating that implanted semiconductors should be annealed up to 2/3 of the melting point for satisfying electrical activation [AMBA98, EDGA94 and ZOLP97].

8.1. Introduction

Nitride-based semiconductor products have attracted considerable attention in the last several years because of their applications in optoelectronics and in high power and high frequency electronic devices [NAKA97]. The fact that GaN has a wide and direct band gap of ≈ 3.4 eV at room temperature makes GaN an excellent candidate material for short wavelength optical devices, especially for violet, and ultraviolet (UV) light-emitting diodes (LEDs), blue laser diodes (LDs) and detectors [MORK94, LEST95, NAKA96 and AKTA95]. Furthermore, GaN could be used in electronic devices such as high temperature, high power, and high frequency transistors. For the manufacture of these optical and electronic devices, high quality GaN thin

film is required [NAKA69]. However, currently most GaN devices are based on GaN thin films grown on substrate such as sapphire (Al_2O_3). Sapphire (0001) has been used as substrates for GaN thin film growth [MARU96, MARU03] because of their ready availability. Nevertheless, it is difficult to grow high quality GaN thin films on sapphire substrate with smooth surfaces because of the large mismatch in lattice constants and thermal expansion coefficients between GaN and sapphire [MORK94, AMAN88]. As a result, there was an urgent need to find a suitable substrate to replace sapphire for the growth of high quality GaN devices.

Akasaki and Amano [AKAS89, AMAN86] has achieved great success to overcome the lattice mismatch between GaN and sapphire using the two-step growth technique. In the two-step growth technique, a buffer layer (AlN) is grown at lower temperature between the GaN layer and sapphire. AlN buffer layer was considered to be the best choice for GaN film growth because of the lattice constant of AlN. However, Li et al. [LI99] found that a GaN buffer layer is more suitable and more efficient, where the processing needs only a decrease of temperature. In 1997, others like Hellman et al. [HELL97] were the first to discuss the possibility of growing GaN on γ-$LiAlO_2$. The (1010) plane of GaN is closely lattice matched with the (100) plane of $LiAlO_2$. In 2000, Waltereit et al. [WALT00] have grown (10$\underline{1}$0)-oriented GaN films by molecular beam epitaxy (MBE) on (100) γ-$LiAlO_2$ substrates.

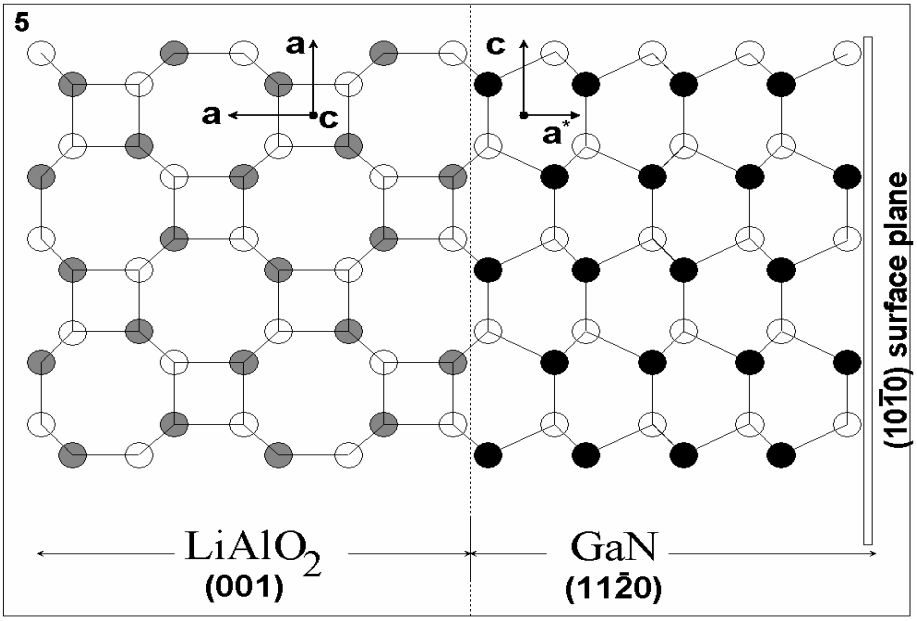

Figure 8.1. A schematic diagram shows a perfect lattice match between $LiAlO_2$ and GaN [MARU03]

Recently, Maruska et al. [MARU03] reported the growth of thick films of GaN (300-400 μm) on γ-$LiAlO_2$ substrates as presented in fig. (8.1). They found that high concentrations of Li and Al on the rear surface of the GaN thin film indicating the diffusion of Li and Al ions from the γ-$LiAlO_2$ substrate into GaN film during growth.

A typical SIMS depth profile of the rear surface of a GaN film grown on γ-$LiAlO_2$ is shown in Fig.(8.2). It can be seen that very high concentrations of Li and Al are present within the first 0.5 μm below the surface of the rear side of the GaN film. To further understand the diffusion of Li ions in GaN, Li ions with different dosages have been implanted into GaN thin film grown on sapphire substrate. These implanted samples were then annealed at several temperatures between

300°C and 1000°C. The re-distribution of Li ions after annealing was studied using secondary ion mass spectrometry technique [FRAN01, FRAN03].

Previous studies have been made on implanted elements into GaN such as the work made by Wilson et al [WILS95] to examine the thermal stability of eight different dopants implanted into GaN thin films. They found that for Be, C, Mg, Si, Zn, and Ge, the implanted dopant profiles do not change after 800°C anneal. For S, or Se, it was found that their profiles started to redistribute after 600°C, or 800°C anneal respectively. The location of the ion-implanted Li in GaN has been studied by Dalmer et al. [DALM98]. They showed that the ion-implanted Li mainly occupied interstitial sites in the center of the c-axis hexagons. This result agreed with the well-known knowledge that Li is a fast interstitial diffuser in most semiconductors.

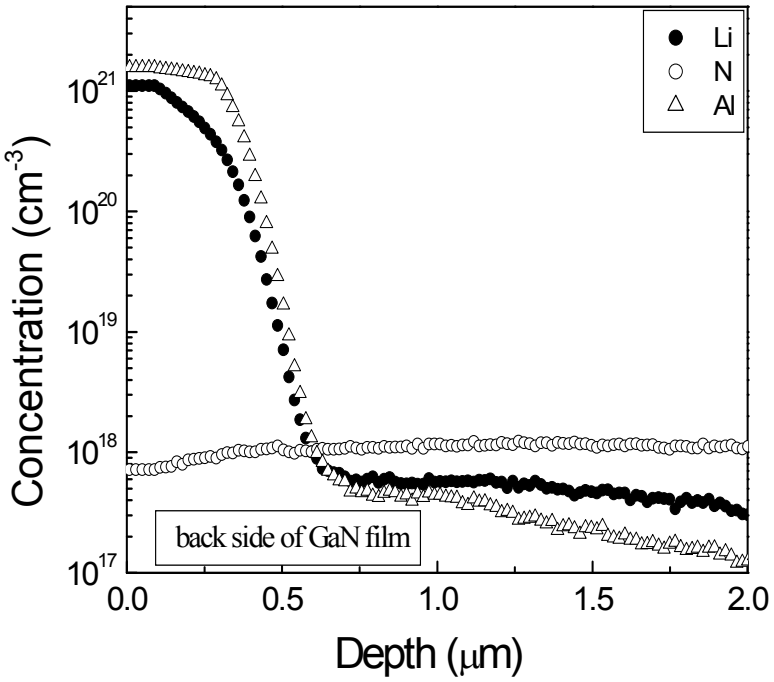

Figure 8.2. SIMS depth profiles of Li, N and Al ions implanted into a GaN film from the back side.

8.2. Experiment

The GaN thin film was grown on a 2.0″ diameter sapphire wafer using a halide vapor phase epitaxy system [MARU03] at Crystal Photonics. After deposition, the wafer was cut into 4 pieces then separately, ion-implanted with Li ions of different dosages: $2.6x10^{12}$, $2.6x10^{13}$, $2.6x10^{14}$, and $2.6x10^{15}$ cm^{-2}. The implantation was carried out at room temperature with an-implantation energy of 90 keV. Thermal anneals were performed for the implanted samples in the temperature range 300 – 1000°C for 30 minutes each. Thermal annealing was carried out as

mentioned previously. SIMS has been used to analyze and characterize the concentration-depth profiles.

8.3. Results and Discussion

Fig. (8.3) shows the depth profiles of the as-implanted Li ions at four different dosages. At $2.6x10^{12}$ cm^{-2} dosages, the Li concentration at the surface of the film is about $2x10^{16}$ cm^{-3} and gradually increased to a maximum of $9x10^{16}$ cm^{-3} at a depth of 0.38 μm. The Li concentration then drops to ≈ 10^{14} cm^{-3} at a depth of 1.5 μm. At $2.6x10^{13}$ cm^{-2} dosage, the shape of Li distribution is very similar to the result from a $2.6x10^{12}$ cm^{-2} implanted sample. Specifically, the concentration peak remains at 0.38μm beneath the surface and its magnitude is about $9x10^{17}cm^{-3}$. As we go deeper into the film, the Li concentration gradually drops to ≈ 10^{14} cm^{-3} at a depth of 1.5 μm, which is the same as that at $2.6x10^{12}$ cm^{-2} dosages. This value of 10^{14} cm^{-3} Li concentration is the detection limit of Li ions for our instrument.

At $2.6x10^{14}$ cm^{-2} dosages, the shape of the as-implanted Li ion distribution in GaN is very different from that at other dosages. As shown in fig. (8.3), the full width at half maximum (FWHM) is clearly wider than the widths at the other three dosages. In addition, there exists a clear "shoulder" (or "bump") at depth between 0.7 to 1.3 μm. We noticed that the Li concentration at this "bump" is even higher than the implant sample at $2.6x10^{15}$ cm^{-2} dosages. The Li concentration eventually drops to 1 x 10^{16} cm^{-3} at a depth of 1.5 μm.

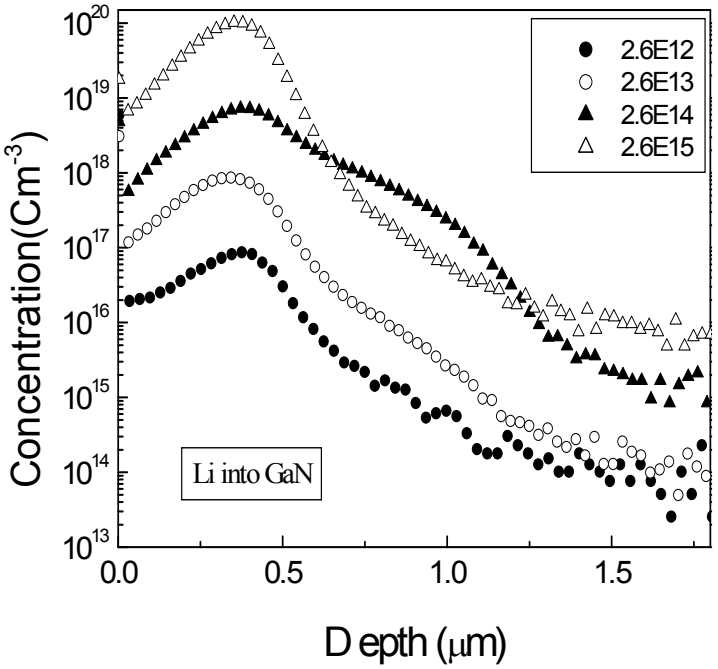

Figure 8.3 SIMS depth profiles of several dosages of Li ions implanted with 90 keV into GaN film grown on sapphire substrate. ($2.6x10^{12}$, $2.6x10^{13}$, $2.6x10^{14}$ and $2.6x10^{15}$ atoms/cm^2).

At $2.6x10^{15}$ cm^{-2} dosages, the shape of the Li distribution follows the Li profiles obtained at $2.6x10^{12}$ and $2.6x10^{13}$ cm^{-2} dosages. At this high dosage, the Li background concentration at a depth of 1.5 μm is about $1x10^{16}$ cm^{-3}, which is about two orders of magnitude higher than the Li background concentrations at the same depth but at lower dosages.

It is not clear why the Li distribution at $2.6x10^{14}$ cm^{-2} dosages is different from the Li distributions at other dosages. One reasonable explanation would be that there was some kind of channeling effect during that particular implant that results in a deeper penetration of the Li ions and a broader FWHM.

The Li profiles in GaN at dosage $2.6x10^{12}$ cm^{-2} as-implanted and annealed at 300°C, 500°C and 700°C is shown in fig. (8.4). There were two abnormal features worth noticing. One was the uphill diffusion of Li in GaN. At 300°C anneal, the peak position of the Li distribution moved 0.04 μm toward the surface. At 500°C anneal, the Li peak concentrations, moved 0.06 μm toward the surface. At 700°C, the peak position of the Li distribution moved 0.08 μm toward the surface. This type of uphill diffusion has been observed in implanted Mg profile in GaAs [ROBI92] in the past. The other unusual feature of the Li profiles in Fig. (8.4) is the out-diffusion of Li ions near the surface. The out-diffusion of implanted Be in GaAs has been studied before [BARA90]. This out-diffusion of Li ions generated a high Li concentration near the surface. The two main reasons for this behavior could be: (a) surface damages acted as sink for the Li ions and (b) the low solubility of the Li ion in GaN.

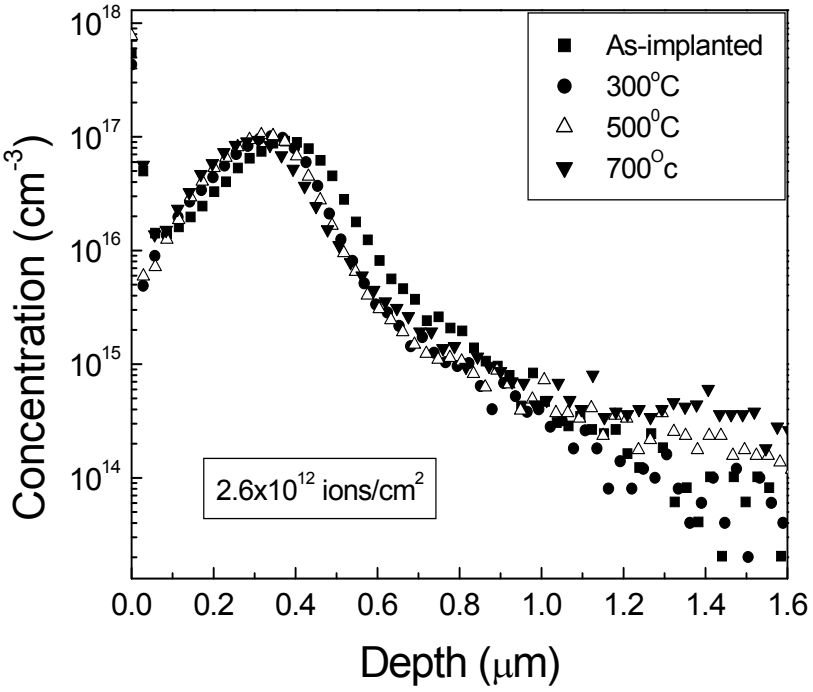

Figure 8.4 SIMS depth profiles of Li $2.6x10^{12}$ atoms/cm^2 into GaN thin film for as implanted and annealed samples for 30 minutes.

Fig. (8.5) presents the Li profiles of implanted Li ions at $2.6x10^{13}$ cm^{-2} as-implanted and annealed at 300ºC and 500ºC. The size of the sample at this dosage was quite small. Therefore, we only annealed at two different temperatures. Our results indicated that Li profiles seem to remain almost unchanged after 300ºC and 500ºC anneals. The only minor change in the concentration occurred in the depth range from 0.6 μm to 1.0 μm.

Fig. (8.6) illustrates the Li profiles of implanted Li ions at $2.6x10^{14}$ cm^{-2} as-implanted and annealed at 300ºC, 500ºC, 700ºC and 900ºC. At 300°C anneal, the diffusion behavior is very

similar to the diffusion behavior in Fig. (8.3), i.e. the profile remained the same except for an increase in Li ions in the depth range of 0.6 μm to 1.0 μm. At 500°C anneal, the Li ions distribution almost remained unchanged. As the anneal temperatures increased, the Li diffusion behavior was very similar to that at lower dosages. In particular, the up-hill diffusion of Li ions can be seen very clearly.

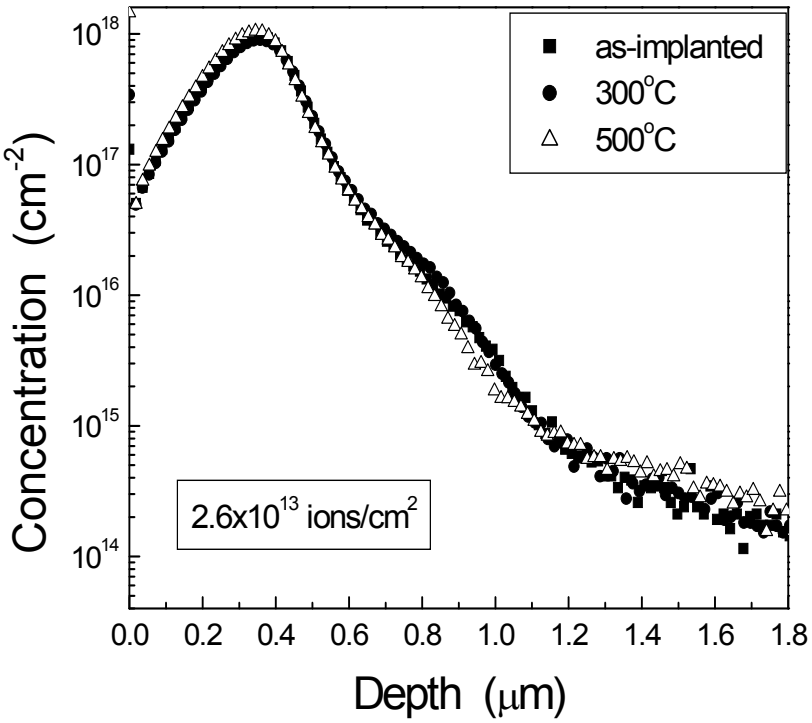

Figure 8.5 SIMS depth profiles of Li 2.6×10^{13} atoms/cm^2 into GaN thin film for as implanted and annealed samples for 30 minutes.

The Li peak concentration actually increased [BARA90] and the full width at half maximum decreased after 700°C anneal. At 900°C anneal, the Li concentration peak moved toward the surface.

We also noticed some Li in-diffusion at a depth of 1.8 μm, i.e. as-implanted and low temperature anneals (< 600°C) showed a Li concentration of $2x10^{15}$ cm^{-3} at 1.8 μm, while the high temperature anneals (>600°C), the Li background increased five-fold to $1x10^{16}$ cm^{-3} at the same depth. At our highest dosage, $2.6x10^{15}$ cm^{-2}, the Li diffusion behavior is dominated by out-diffusion at high temperature anneals (> 800°C) as shown in Fig. (8.7). After 900°C anneal, the Li distribution becomes flat at $1x10^{19}$ cm^{-3} from a depth of 0.2 μm to 0.4 μm below the surface. Near the surface, the Li concentration increased to $1x10^{21}$ cm^{-3}. The Li profiles beyond the projected range inside the GaN (0.5 μm to 1.2 μm) showed some up-hill diffusion as the Li concentration in this region decreased after high temperature anneals. The Li background concentration at 1.8 μm changed from $5x10^{15}$ cm^{-3} at low temperature anneals to $1x10^{16}$ cm^{-3} after high temperature anneals. This may be due to the high peak concentration of Li in this sample. There is a limit of the dynamic range of 10^4 to 10^5 because of resputtering events from the cover plate immediately in front of the first lens (immersion lens).

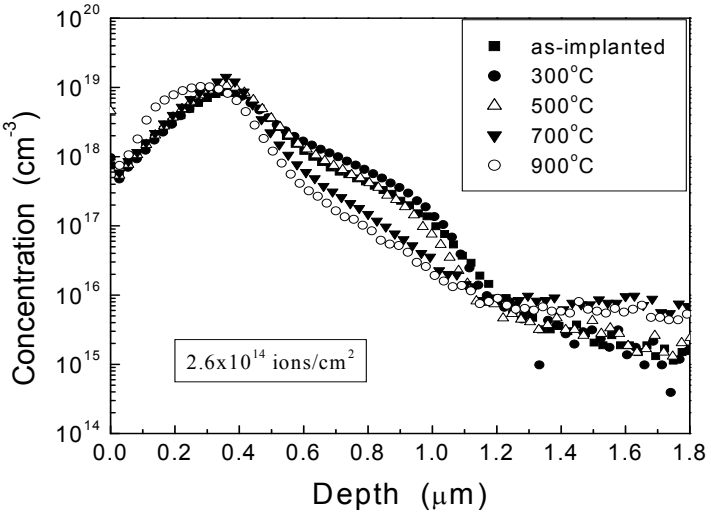

Figure 8.6 SIMS depth profiles of Li 2.6×10^{14} atoms/cm^2 into GaN thin film for as implanted and annealed samples for 30 minutes.

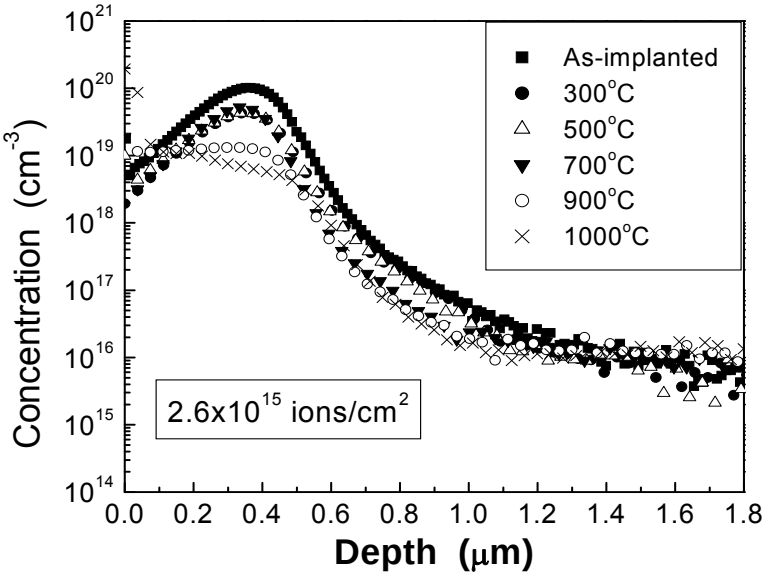

Figure 8.7 SIMS depth profiles of Li 2.6×10^{15} atoms/cm^2 into GaN thin film for as implanted and annealed samples for 30 minutes.

8.4. General Conclusions

Secondary ion mass spectrometry (SIMS) provides an excellent tool to study the as-implanted and annealed Li distribution in GaN thin films. We found that implanted Li diffusion behavior in GaN is complicated due to the interaction between Li and the defects created by ion implantation.

At low temperature anneals (<500°C), up-hill diffusion dominated the Li profiles and at high temperature anneals (>600°C), out-diffusion dominated the Li profiles. The Li background concentrations at 1.8 μm for high implant dosages (>$1x10^{14}$ cm^{-2}) indicated that a small percentage of Li ions acted as fast diffusers.

8.5. References

[AKAS89] I. Akasaki, H. Amano, Y. Koide, K. Hiramatsu, and N. Sawaki, J. Crystal Growth **98**, 209 (1989).

[AKTA95] O. Aktas, W. Kim, Z. Fan, A. Bothkarev, A. Salvador, S. N. Mohammad, B. Sverdlov, and H. Morkoc, Electron. Lett. **31**, 1389 (1995).

[AMAN86] H. Amano, N. Sawaki, I. Akasaki, N. Sawaki, Appl. Phys. Lett. **48**, 353 (1986).

[AMAN88] H.Amano, K. Hiramatsu, and I. Akasaki, Jpn. J. Appl. Phys. **27**, L1384 (1988).

[AMBA98] O. Ambacher, J. Phys. D: Appl. Phys. **31**, 2653 (1998).

[BARA90] H. Baratte, D. K. Sadana, J. P. de Souza, P. E. Hallali, R. G. Schad, M. Norcott, and F. Cardone, J. Appl. Phys. **67**, 6589 (1990).

[DALM98] M. Dalmer, M. Restle, U. Vetter, H. Hofsass, M. D. Bremser, C. Ronning, R. F. Davis, U. Wahl and K. Bharuth-Ram, J. Appl. Phys. **84**, 3085 (1998).

[EDGA94] J.H. Edgar (ed.), Group III Nitrides, London, INSPEC (1994).

[FRAN01] H. G. Francois, E. Anoshkina, F. Stevie, L. Chow, K. Richardson, and D. Zhou, J. of Vacuum Sci. & Technol. B **19**, 1769 (2001).

[FRAN03] H. G. Francois-Sanit-Cyr, F. Stevie, J. M. McKinley, K. Elshot, L. Chow, and K. Richardson, J. Appl. Phys. **94**, 7433 (2003).

[HELL97] E. S. Hellman, Z. Liliental-Weber, and D. N. E. Buchanan, MRS Internet J. Nitride Semic. Res. **2**, 30 (1997).

[KING98] S.W. King, J.P. Barnak, M.D. Bremser, K.M. Tracy, C. Ronning, R.F. Davis, R.J. Nemanich, J. Appl. Phys. **84**, 5248 (1998).

[LEST95] S. D. Lester, F. A. Ponce, M. G. Craford, and D. A. Steigerwald, Appl. Phys. Lett. **66**, 1249 (1995).

[LI99] S. Y. Li and J. Zhu, J. Crystal Growth **203**, 473 (1999).

[MARU03] H. P. Maruska, D.W. Hill, M. C. Chou, J. J. Gallagher, and B. H. Chai, Opto-Electronics Review **11**, 7 (2003).

[MARU96] H. P. Maruska and J. J. Tietjen, Appl. Phys. Lett. **15**, 327 (1996).

[MORK94] H. Morkoc¸, S. Strite, G. B. Gao, M. E. Lin, B. Sverdlov, and M. Burns, J. Appl. Phys. **76**, 1363 (1994).

[NAKA91] S. Nakamura, Y. Harada, and M. Senoh, Appl. Phys. Lett. **58**, 2021 (1991).

[NAKA96] S. Nakamura, M. Senoh, S. I. Nagahama, N. Iwasa, T. Yamada, T. Matsushita, H. Kiyoku, and Y. Sugimoto, Appl. Phys. Lett. **68**, 2105 (1996).

[NAKA97] S. Nakamura and G. Fasol, The blue Laser Diode-Gallium-Nitride based light Emitters and laser (Springer, New York, (1997).

[ROBI92] H. G. Robinson, M. D. Deal, G. Amaratunga, P. B. Griffin, D. A. Stevenson, and J. D. Plummer, J. Appl. Phys. **71**, 2615 (1992).

[VART96] C.B. Vartuli, S.J. Pearton, C.R. Abernathy, J.D. MacKenzie, E.S. Lambers, J.C. Zolper, J. Vac. Sci. & Techn. B **14**, 3523 (1996).

[WILS95] R. G. Wilson, S. J. Pearton, C. R. Abernathy, and J. M. Zavada, Appl. Phys. Lett. **66**, 2238 (1995).

[ZOLP97] J.C. Zolper, S.J. Pearton, J.S. Williams, H.H. Tan, R.J. Karlicek, R.A. Stall, Mater. Res. Soc. Proc. **449**, 981 (1997).